HHS Public Access

Author manuscript

Curr Top Dev Biol. Author manuscript; available in PMC 2021 January 01.

Published in final edited form as:

Curr Top Dev Biol. 2020 ; 136: 271–317. doi:10.1016/bs.ctdb.2019.11.013.

Convergent Extension in the Amphibian, *Xenopus laevis*.

Ray Keller,

Department of Biology, University of Virginia, Charlottesville, VA 22904

Ann Sutherland

Department of Cell Biology, University of Virginia, Charlottesville, VA 22904

Abstract

This review is a comprehensive analysis of the cell biology and biomechanics of Convergent Extension in *Xenopus.*

Keywords

Convergent Extension; Gastrulation; Xenopus

1. Introduction:

The *Xenopus* embryo is an excellent system for analysis of Convergent Extension (CE). Its size and mechanical properties are unmatched for making grafts, recombinants and explants of tissues, which allow high resolution imaging, testing physiological and mechanical interactions of cells and tissues, distinguishing active movements from passive ones dependent on or modulated by mechanical linkages to other tissues, and for revealing emergent properties of the "Mechanome" that shapes the embryo (1). *Xenopus* displays variants of CE involving an epithelial layer and one to several layers of deep (inner) mesenchymal layers, a tissue organization that presents a broad range of mechanisms for analysis.

CE is the convergence (narrowing) of a tissue coupled with its extension (elongation) in an orthogonal axis (2). CE is a kinematic description of tissue deformation (strain) without specifying the force (stress) producing it, as those may be internally generated forces ("active" CE), external forces from mechanically linked tissues ("passive" CE), or some combination of the two. CE is a tissue level description, although in use, the term often assumes or implies a particular cellular mechanism, namely, cell intercalation. However, CE may be driven or modulated by cell shape change (3), oriented cell division *without* growth (4), cell division with growth (5), or some combination thereof. Convergence can also be coupled differently (Section 3), or completely uncoupled from extension (6). In early *Xenopus* embryos cell division is not accompanied by growth and the total cellular volume remains nearly constant (7), the exception being the swelling of notochordal cells due to expansion of intracellular vacuoles after neurulation, which can contribute to extension (8).

Contacts: RK Phone 434-825-2025 434-825-2023 (Cell) 434-823-1975 (home) 434-243-2595 Office.

2. Active, force-producing CE occurs in presumptive notochordal and somitic mesoderm and in presumptive hindbrain-spinal cord during gastrulation and neurulation.

Vital dye mapping (8, 9), as well as tracing cells with fluorescent dextrans (11–13) and with time-lapse imaging (14–17) show that the presumptive notochordal, somitic, and mesendodermal tissues of the Involuting Marginal Zone (IMZ) and the presumptive hindbrain and spinal cord tissues in the Non-Involuting Marginal zone (NIMZ) of *Xenopus* undergo CE during gastrulation and neurulation. CE of these tissues closes the blastopore and elongates the future body axis in one stroke (Fig. 1A–D), and shapes the future vertebral column, the hindbrain and the spinal cord (18) (Fig. 1D–E). The vegetal endoderm and ventral mesoderm undergo CE in early tailbud stages, which straightens and further elongates the embryo (19,20) (Fig. 1D–E). Tracing cells labeled with first generation fluorescent dextrans (21) showed that CE of the presumptive notochordal and somitic mesoderm (11) and hindbrain/spinal cord (12) occurs by mediolateral (across the emerging body axis) intercalation of cells to form a narrower, longer array in both the multilayered deep, mesenchymal region and in the superficial, epithelial layer of these tissues (Fig. 1B–D). Time-lapse imaging showed that the epithelial cells, despite being connected by a circumferential, apical junctional complex, intercalate to form a narrower, longer array during CE (14). This concept of epithelial cell rearrangement was pioneered by work on *Drosophila* imaginal disc eversion by Fristrom and others (21–23).

"Sandwich explants", adapted from Schechtman (25), showed that presumptive notochordal/somitic mesoderm and spinal cord/hindbrain of the IMZ/NIMZ undergo CE while unattached to a substrate and independent of other force-generating processes in the embryo (26) (Fig. 1F, G–H). In explants, mesendodermal and neural regions undergo CE in series, in opposite directions, and of opposite polarity, as indicated by patterning of cell behavior and anterior-posterior (A-P)-specific markers (27, 28), rather than in parallel, the former beneath the latter, as *in vivo* (cf. F-H to B-D, Fig. 1). The "sandwiches" provide a covering epithelial layer, which prevents an abnormal tissue thickening, driven by deep cell surface tension (Section 16; 29), and it shields the deep cells from the culture media which at the time were inadequate for vigorous deep cell motility. These results suggested that these tissues are stiff and can push (generate a compressive force). Uniaxial, compressive stress relaxation tests with the "Histowiggler", an early computer-controlled mechanical measuring device, showed that these tissues stiffen by a factor of 3 to 4 in the axis of extension but not in the axis of convergence, at the onset of CE (30), and they can also push with a force of about a micro-Newton (31). These studies paved the way for deeper analyses of the mechanical properties underlying CE (32), and raised questions of whether the deep mesenchymal layers, the epithelial layer, or both, generate the forces driving CE (Section 15).

3. CE is driven by both radial intercalation (RI) and mediolateral intercalation (MI) of cells.

To image cell intercalation, "open-faced" explants (made from half the sandwich preparation, thus leaving the deep cells exposed, Fig. 1F–I) were lightly compressed

between two coverslips, one forming the imaging interface and the other supported on high vacuum silicone grease (Fig. 1F, I–J) (17, 33–35), a restraint that permits CE but limits thickening due to the tissue surface tension mentioned above (29). Too much pressure increases friction, which retards CE, in extreme cases resulting in tissue differentiation *in situ* without normal movement (see 36). All explants with exposed deep cells were cultured in "Danilchik's Solution" (37), which mimics the ionic composition of the blastocoel fluid (38), supports vigorous deep cell motility, and contains 0.1% BSA to prevent attachment to the coverslip, thus allowing CE (Fig. 1I–J). These explants are made from early to mid-gastrulation and imaged shortly thereafter (17, 34, 35), and for later gastrula (Stg 11-13) and neurula stages (Stg 14-18), "Dorsal Isolates" (32) or "Wilson Explants" (15,16, 33) were made by excising the neural plate with underlying mesendoderm (Fig. 1C–K) and removing the mesendodermal epithelial layer, which allowed imaging the dorsal notochordal and somitic mesoderm (see Fig. 1L).

Low-angle epi-illumination of deep mesodermal tissue in the gastrula (open-faced, Fig. 1I–J)(17) and neurula stages (Fig. 1L) (15, 33) showed directly that CE occurs by intercalation of cells along the axis perpendicular to the plane of the tissue (designated as "radial intercalation", RI), thereby producing tissue thinning (Fig. 2A)). This intercalation was biased to occur between anterior-posterior neighbors, thus contributing to the A-P extension component of CE (Fig. 2B). Deep mesodermal cells also intercalate between one another across the emerging body axis, designated as "mediolateral intercalation" (MI) to form a M-L narrower and A-P longer array (15–17, 34, 35), as predicted by the tracing of contiguous, labeled patches of cells above (Fig. 2C).

The evidence argues that MI and RI act orthogonally, MI producing mediolateral tension and RI producing radial tension, and thus tissue compression in these axes. First, the structure of the IMZ reveals cells and their protrusions in both planar and radial orientations, which–likely generate compressive forces along these axes (Fig. 2D, E–G, Section 4). The relative magnitude of each determines the specific patterns of extension in the A-P axis and thickening or thinning in the D-V axis for a given amount of convergence in the M-L axis, much like elongating a loaf of bread dough involves forces from side-to-side and top-to-bottom (Fig. 2H). The amount of thickening and extension resulting from a given amount of convergence is a tissue specific property, with the notochord extending more and thinning less compared to the somitic mesoderm which extends less and thickens more (15–16) (Fig. 2H). Second, embryos and explants undergoing CE show cells extending protrusions, and putatively exerting traction and generating tension both mediolaterally and radially (magenta and green, respectively, Figs. 2D, E, F, G (16, 39, 40). Third, blocking radial and mediolateral forces independently would be revealing, but both are affected by the same pathways in frogs (41, 42). However, in the mouse embryo blocking MI, and therefore the convergence force, by knocking out Ptk7, revealed a vigorous radial force previously unsuspected because the somitic mesoderm normally thickens; this force dramatically thins and widens presumptive somitic tissue beyond what is normal (43) (Fig. 2H). This suggests that RI and MI, and their resulting forces, act orthogonally to shape axial and paraxial tissues as a function of their relative strengths. Also, failure to display a morphogenic movement, such as thinning, may not indicate absence or failure of the underlying force-generating mechanism, as it may exist but is losing out to larger, opposing forces in the

overall morphogenic system. The embryo is shaped by both regional and global, long-range mechanical forces (44) that comprise the embryonic Mechanome, and further analysis of the mechanical relationship between RI and MI, and their regulation, may go a long way in understanding the specificity of tissue shaping.

4. Mechanisms Underlying the RI Component of CE

The mechanism of RI during CE is less understood than that in the animal cap (AC) where the deep, non-epithelial cells elongate and partially interdigitate along the radial axis (normal to the surface) of the embryo, and then intercalate between one another and contact with the underside of the epithelium to form a single layer of greater area (45). The behavior of excised tissue suggests a model in which the inner layer of deep cells extend protrusions between the intermediate layers to the contact the underside of the epithelium. There they are “captured” by the boundary, and then contract, and wedge between their neighbors, thereby generating a single layer and a compressive, spreading force that produces epiboly (45). The normal, planarly oriented cell divisions that maintain a minimum number of layers are also essential, and both this orientation and RI are dependent on Integrin α5β1-mediated assembly of, and interaction with fibronectin (FN) fibrils on the inner surface of the AC (blastocoel roof) (Fig. 2D) (46). A pathway involving cadherin adhesion, Rac and Pak signaling, the actomyosin cytoskeleton, and the resulting mechanical tension are necessary for FN assembly (47, 48). Planar assembly of FN fibrils is likely essential for RI during CE as well; inhibition of several PCP genes results in abnormal assembly of FN fibrils throughout the radial axis of the mesoderm rather than only at its planar interfaces, and RI and MI are retarded (41). A radial, short range chemotactic mechanism is involved in RI-driven extension of the mesodermal prechordal plate (49) and in the RI driven epiboly of the AC (50). The first involves a mobile isoform of PDGFA and the second involves C3 and its receptor, C3A. The transient or permanent presence of an epithelium, depending on the circumstances, is necessary for CE in the IMZ (15, 17, 33). This epithelium could be a source of a radially polarizing signal driving the radial component of CE; alternatively, it could lower tissue surface-tension, which also contributes to normal CE (51). Computational models of RI suggest “boundary capture” on the underside of the epithelium (50) or the FN layer (52) as an essential element in stabilizing RI. New computational methods are applicable to RI and MI together (Section 10), an advance which may guide experimental investigations of RI-MI interactions (Fig. 2)

5. The mechanism and function of Mediolateral Intercalation Behavior (MIB) in mesodermal CE.

Time-lapse imaging of open-faced explants (Fig. 1F, I–J) and dorsal isolates lacking endoderm (Fig. 1L) showed that MI of deep mesodermal cells occurs by a characteristic “mediolateral intercalation behavior” (MIB), in which initially randomly oriented protrusive activity becomes mediolaterally oriented and bipolar (15–17, 33–35) (Fig. 3). Filo-lamelliform protrusions extend mediolaterally between neighboring cells in a bipolar manner, attach to neighboring cells via C-cadherin adhesions, and contract in the mediolateral axis, thereby pulling themselves between one another in repeated cycles (see

Section 6). MIB appears to be a typical cell-substrate motility, with the exception that cells' "substrate" is one another and the bipolar cells exert roughly balanced traction in both directions (53, 54 and Section 8) (Fig. 3). Expression of MIB is progressive, beginning anteriorly and laterally and progressing posteriorly and medially (Section 12). The notochordal-presomitic boundary forms as function of Eph/Ephrin signaling (55–56; Section 17), beginning anteriorly progressing posteriorly, and thereafter bipolar cells contacting the boundary cease protrusive activity at the boundary end and transition into a monopolar mode with inwardly directed protrusive activity (34, 35). As, or shortly after it forms, fibronectin (57) and fibrillin (58) are assembled into fibrils in the boundary, and are essential for notochord cell intercalation and stabilization of the boundary (59). After the boundary forms, the notochordal and somitic modes of RI, MI, and MIB progressively differentiate as new cell behaviors add to or replace MIB, such as columnarization and thickening in the pre-somitic tissue (15, 16), and modified polarity, intercalation, and vacuolation to form a fiber-wound hydrostat in the notochord (7, 16). These and other late modifications of the basic mechanism of MIB remain poorly understood (see Section 18).

Many studies in *Xenopus* and other species show that the MIB and the resulting CE of the axial/paraxial mesoderm are dependent on the "non-canonical Wnt"/vertebrate planar cell polarity (PCP) and a number of downstream effector proteins (60–74). The common failure of MIB and CE in the wake of PCP perturbations suggests that, in fact, MIB is a major driving force for mesodermal CE in *Xenopus* and other chordates as well, although there is much variation in MIB itself and in its deployment across species. In *Xenopus* the PCP pathway is necessary but not sufficient for polarization during CE. Polarization requires integrin α5β1-fibronectin signaling, as blocking integrin function alone results in expansion of protrusive activity all around the cell, and super-activation of integrins results in suppression of all protrusive activity (75).

6. The Node and Cable Network (NCN) and iterated actomyosin contraction is the "power stroke" of MIB

The polarized extension of protrusions and their adherence to medial and lateral neighbors sets up the "power-stroke" of MIB, which is the cell shortening and resulting traction on the adherent, neighboring cells that pulls the cells between one another and transmits tensile force across the mediolateral aspect of the tissue. This force is generated by a contractile, mediolaterally oriented actomyosin cytoskeleton organized as a Node and Cable Network (NCN) (75–76) (Fig. 3A, B). The NCN consists of actin cables connected to one another at internal nodes to form a network, and to neighboring cells by C-cadherin adhesions (see below), thereby forming a contractile system spanning many cells (76, 77) (Fig. 3C). The contractile activity of the NCN, as indicated by the major displacements of the internal nodes, the C-cadherin adhesions, and the shortening of the cables, is biased toward being parallel to the mediolateral axis of the tissue (Fig. 3C). These contractions are dependent on myosin heavy chain IIB (MHC-IIB) and regulation by the Myosin Regulatory Light Chain (MRLC) in a dose dependent fashion (76, 77). Knock down of Myosin IIB (76) or MRLC activity (77) resulted in decreases in the measured mediolateral convergence force and failure of axial/paraxial elongation and blastopore closure.

Time-lapse imaging of the dynamics of fluorescently labeled C-cadherin and the actin cytoskeleton shows a coordinate development of cell-cell adhesions and contraction of the actin cytoskeleton during intercalation. This suggests that C-cadherin-mediated Cell-on-Cell (CCT)3traction is a major mechanism for transmitting the force generated by the actomyosin cytoskeleton across the mediolateral aspect of the tissue (77). Fluorescently labeled C-cadherin appears as puncta throughout cell perimeter and as larger plaques at lamellipodia. As the F-actin of the lamellipodia flows toward the center of the bipolar cell, it coalesces into a “proto-nodes” and the C-cadherin plaques elongate parallel to and colocalize with the distal actin cytoskeleton, which mature into the definitive nodes and connecting cables. Neighboring cells expressing red or green fluorescent C-cadherin show colocalization in adhesions. Measuring the displacement of proto-nodes and adhesion sites in neighboring cells is consistent the with the idea that the contractile actin cytoskeleton of individual cells is linked into a transcellular mechanical unit by C-cadherin adhesions (77). These adhesions are used to exert traction on other cells and at the same time to serve as contractile (active) substrates for other cells (Fig. 4C). The NCN constitutes a global system of dynamic contractile elements, constantly remodeled with formation of new adhesions and loss of old ones as a function of new protrusive activity, contact and adhesion during rapid intercalation, thereby transmitting tensile force across the entire tissue (43) (Fig. 3C, D. These findings are consistent with pioneering work showing the importance of regulated activity of C-cadherin in CE (78).

Integrating the punctuated actin dynamics described by Kim and Davidson (79) and actin dynamics of the NCN described by Pfister and others (77) argues for a model in which the iterated contractile, condensation of an F-actin network constantly remodels the NCN to reflect the turnover dynamics of C-cadherin adhesions, which in turn are pre-patterned by the polarization of protrusive activity. Defined, quantified, single, iterated cycles of actin concentration in the mid-cell region, as measured by moe-GFP intensity, were strongly and inversely correlated with cell area (79). These “punctuated F-actin contractions” occur in several cell types but in the dorsal mesoderm the contractions were more frequent, moved larger distances, and they were aligned with the long axis of the cell, as the cells became progressively more elongated during CE in the second half of gastrulation. Inhibitor and FRAP studies showed that actin polymerization and F-actin contraction were involved in the punctuated F-actin dynamics. Over-expression of the Frizzled receptor, Xfz7 resulted in more persistent and long-lived contractions whereas the expression of a dominant negative Dishevelled, Xdd1 randomized the orientation of the contractions of mesodermal cells, thereby linking the contractions to the non-canonical Wnt/PCP pathway. Each iteration of polarized protrusive activity results in “new grips”, new C-cadherin adhesions to other bipolar cells. These nascent C-cadherin plaques are enlarged and reinforced with the retrograde/centripetal movement and contraction of the actomyosin network (77), thereby serving as anchorages for the contraction-driven compaction of actomyosin network into the cables of NCN (76, 78). In short, each iterated contraction “scans” for and integrates the retrograde flow of actin from C-cadherin anchorages. Analysis of the change in lengths of cables connecting a series of nodes and adhesion sites across several cells revealed combinations of contractions (shortening), stasis (no change in length), and relaxation (lengthening) of these cables over time (77). These observations suggest ongoing variation

in contractile force of these elements across many cells, with the overall tension of the intracellular-transcellular system being a function of the weakest link. The contractile array is not static but constantly remodeled on a time scale of seconds, and the tensile paths across the multicellular array are constantly remodeled as geometry of the NCN reflects the integration of newly made adhesions and the loss of old ones, always self-aligned mediolaterally by the mediolateral polarization of the protrusive activity protrusion-associated C-cadherin adhesions (77) (Fig. 3C).

7. Cell-on-cell traction rather than cell on matrix traction generates most of the tissue-level, tensile forces driving cell intercalation.

The intercalating deep mesodermal cells also make adhesions with and exert traction on a flexible, fibrillar, fibronectin network assembled between the inner surface of the ectoderm and the outer surface of the mesoderm, a tissue boundary designated as Brachet's Cleft (Fig. 2D) (80). In fact, α5β1 integrin-mediated adhesion to FN, and tension generated by the actomyosin cytoskeleton are both necessary to assemble this matrix, as observed directly by time-lapse imaging of fluorescently labeled fibrils in living tissue (80), suggesting the hypothesis that cells could use flexible FN fibrils as tensile tethers to pull themselves between one another. However, FN-α5β1 integrin signaling is essential for expression of MIB and for CE (75), making it necessary to test the *mechanical function of fibronectin fibrils independent from fibronectin's molecular, signaling function.* Rosario and others (81) ectopically expressed the 70kd multimerization domain of fibronectin, which acts as dominant inhibitor of fibronectin fibrillogenesis, thereby producing embryos, which lack fibrils but have molecular fibronectin available for the integrin signaling essential for cell polarity. These embryos, and explants made from them, show near normal CE, arguing that the cells exert enough tension on the fibronectin to support multimerization and fibrillogenesis but not enough to play a large role in the generating the tensile forces driving CE. Thus, the bulk of the tractional forces are likely due to cell-on-cell traction via dynamic C-cadherin linkages of the contractile actomyosin cytoskeleton of individual cells. However, cell-matrix, cell-cell interactions, mechanical properties of both are linked in multiple ways and levels that are essential for CE. Cadherin adhesion, tissue tension and non-canonical Wnt signaling regulate fibronectin matrix organization (48), and in turn, integrin-ECM interactions regulate the Cadherin-dependent cell adhesion that is essential for CE (42). These results suggest that the early deep mesodermal cell intercalation is driven by a Cell-on-Cell Traction (CCT) rather than cell-on-matrix traction.

8. Balanced traction, regulation of contraction, and the logic of cell intercalation.

Evidence from an abnormal mode of neural cell intercalation argues that the bipolar, CCT mode of intercalation requires balanced traction in the medial and lateral directions to produce CE. Cells of the deep neural tissue normally show monopolar protrusive activity biased toward the midline. When cultured without underlying mesoderm (and thus lacking a midline), they display statistically bipolar protrusive activity when averaged over time. However, this reflects a repeated switch of their major protrusion, and their displacement,

from lateral to medial and back again. The cells just exchange places, the pattern of intercalation becomes chaotic, and CE is greatly reduced (82, 83). This suggests that balanced traction is essential for an effective bipolar mode and raises the question of how the bipolar deep mesodermal cells maintain this balance. In addition, it indicates that *frequency of neighbor exchanges* does not assure nor is it a measure of CE. CE seems to be first an issue of generating large scale tensile force across the span of the tissue, with cell intercalation being an essential follow up (barring any cell shape change).

Also, how is the contractile activity and the relative strength of the linked actomyosin cytoskeletons of the aligned series of cells spanning the tissue regulated? Myosin IIB knockdown results in failure of blastopore closure and CE in a dose dependent manner (76, 77), as well as a reduction in convergence force (77). Moderate knockdowns of Myosin IIB, result in larger and more rapid shortening and lengthening of the internodal segments of the NCN cables and movements of the nodes, suggesting that IIB may be crosslinking actin in the cables and thus enabling them to carry more tensile stress (76), which may be a specialized function of IIB (84, 85). How are the contractile force, tensile properties, and stiffness regulated across the convergence dimension such that local lesions do not occur? The mean stress (force) produced by CE is 5.0±1.6 Pascal (Pa) but CE is mechanically adaptive and can produce three-fold more force in a stiffer environment (86), and in fact the tissue stiffness increases 8-10 fold during CE (32). The evidence suggests that force production should match mechanical resistance to produce a consistent rate of CE. This implies mechanical feedback and the process appears to be adaptive with mechanical accommodation of force production and stiffness (86). Normally, mesodermal MIB/CE operates in an arc anchored at each end, as a homogeneous process that rarely fails within its domain (43). However, when artificially put in series with the weaker process of CT (see 29) in explants, CE/CT combination as a whole does not accommodate, the weaker tissue stretches and produces a plateau in force generation (44).

9. An epithelial, junction remodeling model of notochordal cell intercalation.

A mechanism of cell intercalation similar to the Epithelial Junction Remodeling (EJR) mode of the epithelial germband of *Drosophila* (Fig. 3E) has been described for *Xenopus* notochord (Fig. 3F) (87, 88). Accumulation of pulsed actin, a specific MRLC, Myl9, a higher concentration of phosphorylated myosin (pMyoII), and increased tension are all found along the elongated mediolateral junctions compared to non-mediolateral junctions (those off axis 20 degrees or greater) (Fig. 3F). These parameters are correlated with junction shortening, which brings the vertices of the cells into contact, followed by "resolution" by expansion of a transverse junction, thus resulting in intercalation (Fig. 3F). The myosin activity is confined to a broad area of the apposing, mediolaterally-oriented, shortening junctions by Sept7 located at cell vertices of mediolateral and non-mediolateral junctions. When Sept7 is knocked down, the high concentration of actin at these vertices is lost, and the higher pMyoll at mediolateral junctions, compared to non-mediolateral junctions, is averaged out. Sept7 is localized at the vertices in a PCP-dependent manner where it forms a barrier to retain the pMyoII, and thus the high myosin activity and greater

tension is localized to mediolateral junctions, compared to the non-mediolateral junctions (87).

As a general model for deep mesenchymal cell intercalation, EJR-based model seemed in conflict with the CCT, and an effort was made to find a consensus of the two (89). However, on deeper examination there is no conflict as the two models address two different stages and modes of cell intercalation. The CCT model emerged from making open-faced IMZ explants of the early gastrula (Stage 10-10.5) and imaging them immediately (17, 34, 35) or making dorsal isolates of the same tissue at mid to late gastrula (Stg 11-11.5 and 12-14) and imaging immediately or soon after (15, 16, 76), with all preparations cultured on non-adhesive BSA-coated substrates. These methods capture the early and mid CE period in which the mesoderm narrows rapidly, the notochord narrowing rapidly from 30-40 cells or more in width outside the blastoporal lip to just over 4 or 5 in width at stage 12.5 and further narrowing to just over two, on average by Stage 14 *in vivo* (16, 40) (Fig. 4A, B). It narrows less than that in open-faced explants, the degree of intercalation depending on the amount of compression with a restraining coverslip (34). The cells are participating in both RI and MI at the same time, and thus lamellipodia, the resulting, tractive cell adhesions, and cell intercalations are orthogonal to one another (Fig. 2D, E-G; 3D) and therefore present a complex morphology and arrangement of cells, dynamics of protrusive activity and exchange of focal junctions that are incompatible with the EJR Model.

However, this version of the EJR model is in many respects compatible to events at a later stage and constitutes a major advance in understanding a heretofore ignored problem, the transition from the largely-monopolar inwardly directed motility of the midneurula stage notochord to the late stage neurula/tailbud fiber-wound hydrostat (Fig. 4A, B). EJR model arises from explants made at early to mid-gastrula, cultured for a “half a day” (presumably ~ 12hr) at 15-16 C, on fibronectin coated surfaces before imaging, and at this temperature the stage control embryos would be nearing Nieuwkoop-Faber Stage 15-16 (87, 89). At these stages, the notochord *in vivo* has narrowed to 2 side-by-side rows of interdigitated cells, which then proceed to the final stage of spreading their outside “apical aspects” circumferentially, in the transverse plane of the notochord to form an array of cells shaped like “pizza slices”, which are overlapped to form a newly rounded, fiber-wound notochord (8, 16) (Fig. 4B). Scanning Electron Microscopy (SEM) suggest that the dominant protrusive activity at this stage occurs on a broad front comprising the long diagonals of the “slices” as these edges inter-leaf (16) (Fig. 4B). However, in explants cultured from the early bipolar stage onward on rigid FN-coated surfaces, the “pizza slice intercalation” is unlikely to occur, as offering these bipolar cells an external, undeformable substratum would likely result in zero net force on the cells, conditions that greatly retard CE (36). This would account for the very wide notochords and lack of NSBs in these studies. However, making “Wilson explants” (15) or “dorsal isolates” (32) with the endodermal layer removed (Fig. 1C–L) at Stage 16 and culturing them immediately on non-adhesive substrates in Danilchik’s solution could allow imaging of the normal “pizza-slice phase” of terminal notochord cell intercalation. This would also avoid possible unwanted effects of long-term culture on a very stiff substrate of coverslip-bound fibronectin, as substrate stiffness can affect cell differentiation (90, 91), junction formation (92) and cell motile behavior *in vivo* (93).

10. Comparison of the Mesenchymal, Cell-on-Cell Traction (CCT) Model and the Epithelial Junction Remodeling (EJR) Model of Cell Intercalation.

The CCT and EJR models share the concept of an actively contracting cytoskeleton, but they differ in its organization. In the case of CCT, contractile cables in one cell are linked by transient, focal C-cadherin adhesions to cables of other cells, and the cables have two roles; first, they can shorten and exert traction on another cell, and second, they can serve as "substrate cables", maintaining their length or contracting but in either case, serving as "substrate" for the traction of another cell (Fig. 3C). The cables are constantly reorganized as function of newly formed protrusions, the resulting formation of new adhesions, and their engagement with the iterative actomyosin contractions (77, 79). In the CCT model, many different cycles of protrusion, adhesion, and actomyosin contraction occur to bring about any one intercalation event, whereas in the EJR model, actomyosin dynamics are associated with iterated contractions of long continuous apical junctions, often spanning multiple cells in the case of "rossettes, in the pre-"resolution" stage (94) (Fig. 3E). Both models share the concept of "active (contractive) substrates", in the case of the CCT, internal cables connecting any two or more tractive protrusions (as the plasma membrane is a liquid and offers no resistance), and in the case of the EJR the contractile elements are associated with a long region of two plasma membranes bound continuously by a junctional complex, the elements of which must be recycled (95) or passed through vertices (23)).

The concepts of mediolateral and non-mediolateral junctions do not apply in the same way to cells in CCT and in the EJR models, nor is tension associated with them in the same way. Movies of CCT show cells to be generally fusiform but oscillating from rotund to elongate shapes, generally aligned mediolaterally, and shearing past one another, sometimes as individuals and sometimes as multi-cellular chains (34, 35, 77). As they move by one another their apposed sides give the illusion of a "shortening" junction whereas in reality it is a shear zone. In contrast, the EJR model deals with the continuous "weld" of the apical junctional complex, rather than the C-Cadherin "spot welds" of deep mesodermal cells. As a consequence, the EJR model defines higher tension, shortening mediolateral apical junctions in contrast to lower tension, lengthening non-mediolateral apical junctions. In the CCT model there is no such distinction, as generation of tension is not associated with the necessity of removing the components of a circumferential-apical junctional complex from cell boundaries that are shortening and adding them to others that are expanding. In the CCT, turnover of "spot-weld". Turnover of C-Cadherin junctions serve to allow protrusions to "get a new" grip, a new anchorage for the next contraction of the NCN.

Finally, it should be noted that basolateral protrusive activity and CCT is likely used by the basolateral aspect of epithelial cells whereas the EJR is not used in mesenchymal cells, which lack the defining apical junctional complex. Basolateral protrusions are found in intercalating dorsal epithelial cells of the nematode embryo (96), the neural plate epithelial cells of the mouse (74), and in the *Drosophila* germband (97). In all three cases, the intercalation of the deep part of the cell leads the intercalation of the apical part more frequently than the reverse, suggesting that CCT of the basolateral sides may be the dominant force generating machine.

11. Computational models of CE by MIB mediated CCT.

Several computational models of MIB have been created, and two capture many of the essential features (98, 99). In the first, a finite element model, a lamellipodium extends between two cells, filling the entire interface between them, contacts a fourth cell, and then shortens, pulling the extending and the contacted cell toward one another. This step invokes a doubling of the interfacial tension along the protrusion, as it now has double the number of interfaces and thus twice the interfacial tension. In principle, the single, large extension seems a proxy for tension generated by the many, smaller extensions of lamellipodia between two cells, their adherence to one or both, or to the fourth cell, and there by anchoring the iterated cell shortening seen in ex *vivo movies* (79) Using values for tissue viscosity and tension that are reasonable from the literature, the model results in cell intercalation and CE. If the bounding tissues offer no resistance, the cells are nearly isodiametric at the end, whereas if resistance is offered, the cells elongate in the axis of convergence and CE fails; if intermediate resistance is offered, the cells show intermediate CE and cell elongation, which fits with cell shapes seen in *Xenopus* explants undergoing CE with increasing resistance (35).

The second is a Cellular Potts/Glazier-Graner Hogewege model, which explores a number of relevant processes and is closely integrated with experimental data (99). This work discusses a number of models, and the one most relevant here, the Anisotropic Filipodial-Tension Model, models the number, angular distribution, range, frequency of formation and breakage, strength of cell-cell (filipodial) connections. It examines parameters of planar polarization such as misaligned and passive cells (lack filopodia but can be contacted by filopodia) and refractory cells (cannot be contacted). The model shows the inverse relationship of tissue surface tension and filipodial tension, a result confirmed by experimental suppression of CE by increasing surface tension (51), and it explores the predicted effects of filopodial lifetime, range, number of interactions, and angular range. The investigators also evaluate cell contact mediated behaviors, the effects of degrees of misaligned polarization, and the potential effect of mechanical feedback on failed CE under conditions of high misaligned polarization. 3D versions of the model make it useful for analysis of bipolar and monopolar mechanisms of intercalation and orthogonal processes, such as radial intercalation in the presence of mediolateral intercalation. These models best capture the important parameters gleaned from observed behavior of early deep mesodermal cell intercalation (35, 76, 77) and offer an excellent guide for further experimental exploration, including convergence on two axes and extension on the third, and two converging and one extending axis (see Sections 3, 4).

12. Large Scale Patterning of MIB is Essential for Normal CE Function.

Large scale patterning of MIB is essential for mesodermal CE to function in both closing the blastopore in the second half of gastrulation, and in elongating the body axis through neurulation (35, 53, 54). The large-scale patterning in the embryo (Fig. 5A) was described by imaging large open-faced explants comprising most or all of the IMZ (Fig. 5B–D) and mapping the pattern back on to the gastrula. Time-lapse imaging revealed a progressive A-P expression of MIB across the late involuting IMZ. MIB/CE begins at Stage 10.5 two hours

after the onset of blastopore formation in the presumptive anterior somitic mesoderm on both sides of the midline adjacent to the vegetal endoderm, and it proceeds medially toward the midline where the two lateral components meet to form the arc-shaped vegetal alignment zone (VAZ; Fig. 5C, E) (35, 101). As this arc grows in thickness, the notochordal-somitic boundary (NSB) forms within it and progresses the full length of the A-P axis of the body plan to separate the notochordal and somitic mesoderm (Fig. 5C,D). After formation of the NSB, MIB proceeds from A to P in the lateral regions of the presumptive notochordal and presumptive somitic mesoderm (yellow arrows, VE, Fig. 5C, D, E). From this lateral origin, next to the vegetal endoderm in the case of the somitic mesoderm, it proceeds toward the notochord, and in the case of the notochordal mesoderm, it proceeds toward the midline (Fig. 5B–D). Mapped on to the IMZ of the gastrula (Fig. 5A), the A-P progression takes the form of an arc-like pattern that progresses posteriorly in a continuous manner. However, it can be better visualized as discrete hoops anchored on both ends at the vegetal endoderm and arcing across the dorsal IMZ from the presumptive A (darker hoops) to P (lighter hoops). The origin and anchorage of the arc of MIB at the vegetal endoderm in the region of bottle cell formation is particularly interesting. The animal edge of the vegetal endoderm is the source of Nodal signaling (see 102). It is the site of strong mechanical anchorage of the mesoderm to the endodermal bottle cells and thus the vegetal endoderm. It is the transition from the lateral border of the CE-expressing (pre-somitic) mesoderm to the boundary of the directed (collective) migration-expressing head, heart, and lateroventral) mesoderm at the leading edge of the mesodermal mantle (53, 54, 103). Thus, it is a largely uninvestigated nexus of signaling and mechanical importance.

The advancing front of MIB/CE takes as MIB begins at the point of involution and progresses posteriorly from this initiation as the IMZ rolls over the lip. The posteriorward progression probably occurs as a result of a combination of forces. First the straightening effect of the stiffening IMZ tissue (30) undergoing progressive MIB/CE from the inside out might tend to pull the IMZ over the lip. Second, it might be pushed from behind by Convergent Thickening (CT), an isotropic convergence and thickening of the pre-involution IMZ driven by transient increase in tissue surface tension (29). Third, the *tissue separation behavior* (104) must operate to support the posterior lengthening of the Cleft of Brachet, itself a complex process of Eph/Ephrin function downstream of many regulatory inputs (105–108). The mediolateral convergence of IMZ tissue in this arc-like, laterally anchored pattern results in narrowing and lengthening of the gastrocoel/archenteron roof, elongating the dorsal body axis, and closing the blastopore in one stroke. Note that the MIB-driven shortening of the arcs pulls the left and right vegetal margins (where they were attached to the vegetal endoderm i*n vivo)* in an arc back towards the midline, thus producing CE. *In vivo*, however, the ends of the arcs are anchored in the vegetal endoderm and thus their shortening by MIB *pulls the dorsal tissues ventrally, over the vegetal endoderm* until the blastopore is closed. Note also that the degree of CE increases toward the posterior, that posterior parts of the presumptive A-P axes in the notochord and somitic mesoderm (the arrow heads) are brought together as the Limit of Involution converges and closes the blastopore. Lastly, the arcs of convergence are truncated and not continuous with those in the notochord in the lateral and ventral regions IMZ (Fig. 5A). This is because the notochord shears posteriorly with respect to the somitic mesoderm, which shows less extension and is

lengthened, in part, by addition of cells streaming around both sides of the posteriorly moving blastoporal region (15, 16, 33); this posterior shearing acts as a spline or "zipper" that pulls the two sides of the blastorpore together. In the giant explant, the posteriorly moving "front" of activation MIB/CE is at the concave, neck-down point of the explant (Fig 5D), and in the embryo, it lies just inside the blastoporal lip and proceeds posteriorly into the freshly involuting tissue. Again, CT occurs in the pre-involution IMZ, and in the case of the early involuting mesoderm, it transitions into animally-directed migration of head, heart and lateroventral mesoderm, and in the case of the late involuting mesoderm, CT transitions into CE of notochordal and somitic mesoderm at the point of involution (29).

Understanding the A-P patterning of MIB is a fundamental problem. The participating cells do not appear to be strictly predetermined to express MIB at a particular time and place, as labeled notochordal cells from various A-P and M-L regions of the early gastrula scattered randomly by transplantation into unlabeled, host IMZs, adopt MIB in the normal A-P and L-M progressions, although with some delay, suggesting a response to some endogenous, ongoing signaling process (109). The extent and progression of CE in *Xenopus* is dependent on the activity of Nodal and its inhibitor, Lefty (110). Luxardi and others (102) present evidence that distinct *Xenopus* Nodal Related (XNRs) signals act sequentially *in vivo* in two phases. In the early phase, XNR5 and XNR6, acting together, induce mesendodermal tissue differentiation, and in the late phase XNR1 and XNR2 regulate morphogenic movements of gastrulation, including CE, by regulating effector genes *papc, has2 and pdgfra, indepdendent of the Wnt/PCP pathway.* Interestingly, they found that the Wnt/PCP pathway was not regulated by the Nodal pathway, and they propose a parallel regulation in which Nodals activate cell movement effectors and Wnt/PCP polarizes the activities of these effectors.

Graded Nodal signaling along the A-P axis, and the resulting differences in A-P positional identity appear to be necessary for MIB (111); the nature of this positional effect is unknown. Both the L-M and A-P progressions of MIB may require positive feedback. In large explants that are compressed and not allowed to move significantly, expression of MIB fails to reach presumptive posterior midline of the notochordal field nor does it reach the presumptive posterior somitic tissue (35), suggesting that CE potentiates its own progress, perhaps by bringing tissues in the range of the signaling source. Additionally, there appears to be an A-P/early-late discontinuity in the mechanism of MIB regulation, as there is an early critical period before the formation of the VAZ (Stg 10.5) in which microtubules (99) and the activity of a RhoGef (112) are essential for further progress of MIB, but not thereafter.

The geometry and progressive shortening of the hoop pattern of MIB is essential for proper involution and blastopore closure. Inhibition of Lefty, a Nodal feedback inhibitor, results in excessive rate and extent of expression of CE, beyond its usual range, and causes defects in involution and blastopore closure (110). Lithium treatment of the blastula results in activation of the Wnt pathway, expression of "Spemann Organizer" properties, and expression of CE uniformly throughout the entire IMZ, which often results in failure of involution and extension of a proboscis of converging/extending tissue (113). This likely occurs because the asymmetric, vegetally anchored, hoop-like pattern of progressively

expressed MIB in the normal embryo is transformed into a symmetric, concentric pattern, unanchored to the vegetal endoderm, and perhaps showing little or no progressivity of MBI expression. Rapid and symmetric expression of CE would likely result in an outward extension of tissue too stiff to bend over the lip.

The alignment of the elongated fusiform deep mesodermal cells expressing MIB may be related to differences between their A-P surfaces. The PCP protein Prickle (Pk) is enriched on the anterior surface and another, Dishevelled (Dvl) is enriched on the posterior surface (68). The A-P surfaces appear to be important for cell alignment and intercalation; apposition of two notochords in dorsal explants in parallel orientation results in rapid loss of the fibronectin matrix between them and the cells intercalate to form one, longer notochord. In contrast, juxtaposing two notochords in anti-parallel configuration results in loss of matrix and a visible boundary, but cells from opposite sides will not intercalate or mix across the boundary of apposition (113). The difference is that in the parallel orientation, A-surfaces face P-surfaces and in the antiparallel case, A-surfaces face A-surfaces and P-surfaces face P-surfaces. At the ends of the recombinants, the cells reorient, as if they could read A-P positional values. On one end, they turn their A-surfaces facing the A end and their P-surfaces facing the P end, and on the other end they turn the opposite way, but in both cases their A-surfaces now facing P-surfaces of cells the other half, and they intercalate and form axes transverse to the originals (113). These behaviors suggest that anterior and posterior surfaces must face the opposite surfaces of other cells for intercalation to occur. If and how this is related to A-P differences, including the localization of Prickle and Dvl, in frog and other species, is not clear. Also, how do offsets of A-P positional identity regulate expression of MIB (111) Cells in neurula-stage explants show a PCP-dependent oscillatory actomyosin contraction that is out of phase in sequential A-P rows of cells (115). The function of this phenomenon, and whether it occurs in the early phase of deep mesodermal intercalation in the last half of gastrulation-early neurulation is not known.

13. Patterning of mesodermal CE relative to other landmarks and presumptive tissues.

A common misunderstanding is the perception that the tissue around the lateral sides of the blastopore constitutes the “dorsoventral axis”. In fact, it is the physical A-P axis of the somitic mesoderm, and the dorsalization event that occurs along this axis is actually the recruitment of late involuting cells from the ventral side of the blastopore into becoming “dorsal” somitic mesoderm at progressively more posterior levels (13, 15–17; 101, 116–117). The future lateral (or “ventral”) aspect of the somitic mesoderm is at the ends of the arcs of convergence next to the vegetal endoderm and the medial (or “dorsal”) aspect of the somitic mesoderm is next to the presumptive notochordal boundary. The “ventral tissues”, the head, heart and lateroventral mesoderm, lie vegetally in the IMZ, involute early (first) and progressively, in that order, whereas the presumptive “dorsal” mesoderm is in the animal part of the IMZ, involutes late, and forms the notochordal and somitic tissues (103). The early involuting mesoderm at the ventral side of the vegetal endoderm escapes dorsalization as it involutes early, and the late involuting, presumptive posterior somitic tissue lying at the “ventral” side of the blastopore of the midgastrula is subject to dorsalizing signals and

moves around both sides of the closing blastopore, shears along the side of the notochord, and joins the posterior end of the segmental plate as somitic mesoderm *in vivo* (15, 16). In the "giant", sandwich explant, CE proceeds to completion and most of the far ventral (lateral in the explant) regions are swept up into the somitic mesodermal files but in open-faced giant explants, friction retards movement, CE does not go to completion, and only about two thirds of the somitic mesoderm forms (35). It is popular to use the original fate maps (9, 10), perhaps because they better fit simple models of movement and patterning, but the revisions cited above are important changes and better guides going forward.

14. Neural Cell Intercalation and CE.

The neural plate of *Xenopus* undergoes CE in parallel with the underlying mesoderm, matching its behavior quite closely (9, 10, 18). In urodele amphibians, the extension of the neural tissue occurs in large measure by mechanical coupling (attachment) to the underlying, elongating notochord (100), but in *Xenopus* presumptive neural tissue in the sandwich explant shows robust CE without underlying mesoderm (26) (Fig. 1F–H). Neural CE is induced by planar signals emanating from the posterior mesoderm (the Organizer) (27, 28, 118), and the extending neural tissue is patterned in proper A-P order as shown by neural markers (Distaless, Otx2, Krox20, HoxB1, HoxB9) (27, 28). Without contact with the underlying notochord the notoplate/floorplate does not form by molecular markers or by morphology (28, 12). Patches of fluorescently labeled cells grafted into the these extending neural structures *in vivo*, or in explants, are dispersed along the A-P axis with increasing separation with distance posteriorly, indicating progressively greater CE and mediolateral cell intercalation, as in the mesoderm (11). Although the deep mesoderm expresses MIB and CE in open-faced, gastrula explants, the deep neural region does neither in early gastrula, open-faced explants, whereas early neurula deep cell explants do (see below). The gastrula stage deep cells may require mechanical assistance from an actively extending epithelial layer (119) or physiological support.

As in the case of mesodermal CE (Section 5), neural CE in *Xenopus* is dependent on the PCP pathway as is neural tube closure (120–121). Grafts of labeled, normal animal cap into the presumptive neural region of Stage 11 gastrulae results in its induction to form neural tissue and it undergoes CE, neural tube closure, and normal body axis elongation. However, similar grafts expressing XDsh-D fail to show CE, fail to close the neural tube, and the body axis has an extreme dorsally concave flexure, as expected if the neural component failed in extension coupled to the extending mesoderm. Disrupting *Xenopus* Dishevelled (XDsh) with Xdd-1 (affecting canonical and noncanonical Wnt signaling) and XDsh-2 (noncanonical only) results in failure of neural tube closure in half or more of the embryos. Targeting inhibition of XDsh to the medial and lateral parts of the presumptive neural plate showed that is needed for CE but not neural fold formation nor for their medial movement. XDsh inhibition prevented CE of both the midline region and the lateral regions of the neural plate followed XDsh-2 inhibition, but neural tube closure was blocked only by the midline perturbation. The conclusion was that neural tube closure failed because the folds were too far apart due to failure of CE to sufficiently narrow the midline tissue (120–121; also 65). On second thought, a broader neural plate, with more cells across its mediolateral extent, would not necessarily compromise meeting of the folds, since, as with barrel staves, the

more units (cells or staves) there are, the less angle of “wedging” required by each for closing the circle. The PCP pathway also compromises events on the radial axis (42) and apical constriction and cell wedging (122).

The epithelial layer of the *Xenopus* neural plate shows cell intercalation by the ERJ mechanism, through the shortening of mediolaterally oriented junctions and subsequent expansion of non-mediolaterally oriented junctions (119) (Fig. 4A, E). The PCP proteins Prickle2 and Vangl2 were found to be enriched in shortening junctions and depleted in the expanding junctions, corrected for concentration due solely to shortening. FRAP studies revealed that the stable fraction of both proteins was higher in shortening junctions and in proportion to the rate of shortening. Imaging a GFP fusion to the myosin regulatory light chain Myl9 showed enrichment of myosin at the shortening junctions, an enrichment that was lost with expression of inhibitory Xdd1 and P2-ΔPΔL (121).

The deep cells of the neural plate also converge on the midline as the plate narrows, and their behavior can be observed in neural plate explants with the overlying neural epithelium removed (82, 123) (Fig. 1C–N). The notoplate/floorplate differentiates over the underlying notochord in these explants, and with the notoplate present, deep neural cells display a monopolar, medially-biased protrusive activity toward the midline notoplate. When they reach the notoplate-neural plate boundary, they stop and the cells behind them intercalate between their now-stalled medial neighbors and thus contribute to CE of the neural plate (Fig. 4A, D) (123). Cells contacting the notoplate boundary rarely, if ever, leave, supporting a “boundary capture” mechanism as proposed by Jacobson and others (124). This ensures maximum efficiency of intercalation, that is, nearly all the intercalations are productive in producing CE (34). Regulation of this behavior may involve two signals. Removing the midline notochord/notoplate region of a neural plate and abutting an ectopic notochord/notoplate the other side results in the cells near the ectopic notochord expressing the normal monopolarity and orienting toward the ectopic notochord. In contrast, cells farther away express monopolarity but orient toward the “ghost” midline that had been removed, suggesting that a persistent midline signal orients any monopolarized cell in the field. In contrast, monopolarization itself requires a short-lived signal from the midline (125). Testing the notochord and notoplate independently suggests that the notoplate by itself can polarize cells nearby but not farther away, whereas the combination of notochord and notoplate does both (126).

The isolated, explanted deep cell layer of neural plate (Fig. 1O) shows relatively little CE compared to deep neural layer isolated with underlying mesoderm. Live imaging revealed vigorous, bipolar protrusive activity when averaged over time, but at any given time they were monopolar and indecisive, constantly alternating between medially and laterally directed protrusion, displacement, and intercalation, exchanging places with one another rather than intercalating to produce CE (123) These observations underscore, first, that the frequency of neighbor changes, even if oriented, does not necessarily result in CE. CE instead depends more on generating mediolaterally oriented tensile force, which compresses the tissue mediolaterally, and thus brings about convergence, rather than a simple positional exchange. Second, if the bipolar mode is used, traction must be approximately balanced at the two ends at any one time; if it is unbalanced, the cell will simply make cancelling

excursions first one way and then the other. Finally, the unbalanced bipolar mode may be an atavistic behavior, a remnant of a former bipolar mode, elements of which are used for the current monopolar mode and uncovered in its absence. Morphogenic mechanisms are not *de novo*, complete, unitary machines but composites of new elements added to the evolutionarily preceding mechanisms, which have since been modified to their new role in evolutionary time.

15. Forces and Mechanics of the Progressive Expression of Mesodermal MIB.

CE of the notochordal, somitic and the posterior neural tissues close the blastopore and elongate the dorsal side of the embryo in pre-tailbud stages by producing a tensile convergence force and the compressive extension force to accomplish this transformation. “Giant Sandwich Explants” of the entire IMZ/NIMZ mounted in a tensile force measuring device measures the total tensile convergence force of both mesodermal and neural CE (44). Convergence force rises at the onset of gastrulation to 1.5-2.0 μN when it plateaus through the end of gastrulation, and then rises to over 4.0 μN by the tailbud stage. The convergence force generated before Stage 10.5, and thus before the onset of CE, is generated by CT, an active, force-producing process acting in the pre-involution IMZ, as described above (29). At Stg 10.5 (early mid-gastrula), MIB/CE begins but contributes force progressively as the process recruits more cells. The force plateaus temporarily as less stiff lateral tissues undergoing CT, connected to the stronger, stiffer midline region of CE/MIB, begin to stretch. This interpretation is confirmed by the fact that the plateau is lost in older explants having undergone the CT to CE transition, or in dorsal IMZ explants, which lack the intervening CT expressing region (44), thereby directly connecting the CE/MIB region to the force measuring machine. *In vivo*, CE occurs post-involution and is directly connected to the vegetal endodermal boundary region, without an intervening region of CT, which occurs pre-involution *in vivo* (29). It is important that CT and CE occur in parallel, the first outside and the second inside the blastoporal lip, rather than serially, as in the explant, any break in the arc-pattern of MIB/CE results in catastrophic failure of gastrulation (25, 127). Direct connection of MIB/CE in older or dorsal explants probably approximates the *convergence force at the blastoporal lip* but underestimates the *total force along the dorsal axis* generated *in vivo*, however, as both neural and mesodermal tissues extend away from the axis of measurement, they pull on the measuring platters at an increasingly steep angle and thus less efficiently; the same is true *in vivo* with regard to the blastoporal lip, and thus these measurements may approximate that at the blastoporal lip. Force of blastopore closure was measured at 0.5 μN with a dual cantilever device, structural stiffness increased by 1.5 fold (128; also see this work for maps of cellular strain). In summary, the IMZ/NIMZ generates constant tensile convergence force for many hours. The MIB/CE component of this force increases as more cells undergo MIB in parallel, and it is transmitted to the ventral ends of the explant with increasing efficiency as MIB progresses toward the ends (44) Accordingly, morpholino knockdown of Myosin IIB (76) or reduction of MRLC activity (77) results in proportional failure of blastopore closure (76), altered behavior of the NCN-actin dynamics (76, 77), and generation of less convergence force (44).

Early experiments showed that the sandwich explant can push (31) and that the tissues undergoing CE stiffen from about 3 Pa to 10 Pa from the early to mid-gastrula (30). Recent work showed that dorsal isolates, consisting of the complete neural and axial/paraxial mesodermal/endodermal components, stiffen from less than 20 Pa to over 80 Pa from gastrulation to the end of neurulation (Stg 22) (32). This is a key factor in the morphogenesis of this period, as tissue must stiffen in order to push, and the stiffening is more dependent on the cortical actomyosin cytoskeleton than on matrix (fibronectin fibril) assembly in this period (32). These investigations also employed the superposition principle of analysis of composite materials, paired with microsurgical construction of explants of different compositions (normal explants, ones with no notochords, with two notochords, etc), to estimate the relative contributions of the different tissues to embryonic stiffness (32). The results showed that midline tissues are stiffer than lateral tissues, but of the midline notochordal and paraxial tissue, stiffness was the same with and without notochord, and medial paraxial mesoderm adjacent to the notochord was the stiffest tissue. Explants lacking neural tissue did not differ significantly from the whole dorsal isolate but ones lacking endodermal tissue were stiffer, meaning that the endoderm is the weakest tissue (32). Using the composite analysis, these investigators concluded that compared to the dorsal isolate as a whole, the endoderm is the least stiff by 10 fold, the neural and notochordal tissues are similar, and similar to the dorsal isolate as whole, and the paraxial mesoderm is the stiffest at near two fold that of the isolate as a whole. Interestingly, they note that this tissue undergoes major changes in cellular architecture, notably the thickening and formation of the “buttresses” against the underside of the nerual plate, due to a columnarization component to somitic convergence (15, 16), and have been proposed to aid folding of the neural plate (129). However, cell size and tissue architecture seem to make less contribution to the bulk mechanical properties of these embryonic tissues than the cortical actin cytoskeleton (130), and this stiffness, and thus the capacity of the medial paraxial mesoderm to generate an extension force, may be related to the accumulation of pMLC, a regulator of the actomyosin cytoskeleton at the apposed regions of the pre-myocoel surfaces of this tissue (32).

These results suggest that the paraxial mesoderm may be the major contributor to CE forces driving both the convergence and the extension in this period of neural tube closure, a suggestion supported by the fact that isolated pre-somitic mesoderm will show CE whereas isolated notochord does not (14, 33). Other studies using a gel-based force sensor show that the mean stress (force) produced by CE is 5.0+/−1.6 Pa, and again, the notochord is not necessary. By increasing the gel stiffness, they found that dorsal isolates accommodate to the mechanical environment by increasing stress production in stiffer gels (131). In stiff gels, the notochord was curved and mushroomed at the rear, suggesting involvement force generation but again tests of this parameter with and without notochords revealed no difference.

16. Evaluating the Contributions of the Epithelial and Deep Layers to Forces Driving CE.

This issue is complicated by the fact that the two layers may have both signaling and mechanical interactions. Dorsal sandwich explants (Fig. 1B,F,G), in which the epithelial layer is replaced with animal cap epithelium, a region that does not undergo CE,

nevertheless show CE, and so do controls having the native epithelium removed and replaced, but neither do so as well as intact explants (26). This argues that the deep, mesenchymal layer can drive the CE of itself and that of an attached epithelium, which does not normally undergo CE in its native position but does not rule out force generated by the native epithelium of the IMZ when operating *with* its deep layer. The contribution of the epithelium alone, independent of the deep region, could not be evaluated because of the instability of epithelial sheets cultured alone and without adhesion to substrates. CE of early dorsal explants fails on removal of the epithelium early but not later (33), suggesting a transient, early effect, perhaps the radial specification of matrix deposition to particular interfaces (41). In other situations, ongoing contact with an epithelium, either endodermal or ectodermal, is essential for radial intercalation and CE of the somitic mesoderm (16, 33). The epithelial contribution could perhaps be assayed by a composite analysis of mechanical properties (see 32).

Contributions of the epithelial layer may not be due solely to the EJR mechanism of cell intercalation. The epithelial sheets of the nematode (96), the mouse (74), and the *Drosophila* germ band (97) have basolateral protrusive activity, and in all these situations, neighbor exchange, the “resolution” step of the basolateral end of the cells, occurs shortly or substantially before that of the apical region, suggesting that basolateral protrusive activity and cell traction may play the major role in driving epithelial cell intercalation (see below). Epithelial tissues of the *Xenopus* gastrula may use basolateral protrusive activity and cell traction, as the mesodermal, endodermal and ectodermal epithelia of the early embryo have basolateral protrusions (16, 39, 45).

This raises the question of how much tissue-level force the EJR can produce. In the *Drosophila* germband, the initial contraction of the shortening boundary that brings cells to a common vertex (green arrows Fig. 3E, left and middle) is followed by a medial (centripetal) actomyosin contraction in the same cells that elongates the transverse boundary (red arrows, Fig. 3E, middle and left), presumably passively stretching it (black arrows, Fig. 3E, left), and thus accomplishing “resolution” and elongating the array of cells in the orthogonal axis (132). This process normally produces elongated arrays of cells that are aligned in the axis of germband extension, and thus they contribute to the extension, However, if the posterior midgut invagination is prevented, the germband does not elongate properly and the local elongated arrays become misaligned and compressed (132). These results are a welcomed illumination of the mysterious “resolution” step, and they suggest that in this case the EJR functions to remodel apical junctions, but externally generated force, in this case tension produced by the posterior midgut invagination, is required for elongation or CE. This work also suggests that the basolateral protrusions of these particular cells (97) do not generate sufficient force to bring about tissue level CE. The broader question is whether the EJR mechanism functions primarily in remodeling junctions, a necessary component of CE by cell intercalation, but the major stress driving tissue strain during CE is generated by basolateral CCT.

17. The role of tissue boundary formation, Eph/Ephrin signaling, and tissue surface tension in CE.

For CE to occur properly, the boundary properties on all sides of the tissue must be regulated to maintain physical integrity and to manage tissue surface tension (51). As the IMZ involutes, its deep cells come into contact with the inner surface of the blastocoel roof, and they display *tissue separation behavior (TSB)*, meaning that they will not reintegrate with the cell layers they just left. They thus maintain a clear separation boundary, called the Cleft of Brachet between the outer neural ectoderm/epidermis and the inner mesoderm (104). TSB is assayed by placing pre and post involution tissues on the inner surface of the blastocoel roof; the pre-involution ones will reintegrate into the roof, the postinvolution ones will remain separate (104). TSB involves non-canonical Wnt signaling through the Wnt receptor, XFizzled-7, paraxial protocadherin (PAPC), and the ankyrin repeat domain protein 5 (xANR5), and finally, activation of RhoA and Rho kinase (105–108). Ephrin B ligands and EphB receptors signal across the tissue boundary in both directions, resulting in a repeated cycle of transient attraction, attachment, followed by repulsion and detachment. This simultaneously maintains a dynamic tissue contact but permits the shearing between the layers that is essential for mesendoderm migration on the roof of the blastocoel, as well as any differential rates of CE in axial/paraxial mesoderm and neural tissue.

The immediate response to removing pre- and postinvolution tissue from the embryo, as in making sandwich or open-faced explants, is a tissue-surface tension driven reduction in its newly exposed deep cell surface area. This results in thickening, concave curling at its deep surface, and eventually rounding up and thereby retarding CE. On the other, outer side of the deep mesoderm, the overlying endomesodermal epithelial sheet also has the effect of lowering the tissue surface tension of the underlying deep mesoderm. Lowering tissue surface tension appears necessary to allow CE, a process that involves an increase in surface area. Reducing the epithelial properties by co-expression of a dominant negative aPKC and Lgl results in rounding and decreased CE of tissue aggregates by raising their surface tension, and regulating epithelial contact can controls fine modeling of deep mesenchymal tissue shape (51).

Open-faced explants having the native epithelium on one side, but lacking the surface tension reducing effect of tissue separation on the deep side, will thicken immediately on separation and must be restrained from doing so by two non-adhesive glass coverslips (34–35). This is a limitation of open-faced explant system. Culturing open-faced preparations on FN-coated, rigid substrates such as glass or plastic will usually prevent thickening but that comes with a number of problems and uncertainties. It also promotes unregulated and abnormal migration and spreading of inherently migratory cells, probably because of the extreme stiffness of and avidity of the glass or plastic for binding FN. The same properties likely account for the fact that it greatly retards or stops CE of tissues such as somitic mesoderm and notochord, which employ the bipolar intercalation mode, a mode that would be expected to fail to produce interdcalation on an undeformable, adhesive substrate. The extreme stiffness compared to the endogenous flexible fibrillar array, which does thicken and perhaps stiffens over time (80), could result in a number of developmental changes (90–

93). The second convergence movement in gastrulation, CE, involves an increase in surface area and requires a lowering of surface tension, and the first convergence movement in gastrulation, CT, involves decrease in surface area and is driven, at least in part, by an increase in tissue surface tension due to loss of affinity of the deep mesenchymal IMZ for the overlying mesendodermal epithelium (29).

18. Late elongation and straightening of the body plan is driven by notochord straightening and elongation, and elongation of the vegetal endoderm.

In the early neurula stage, mediolateral intercalation brings the notochord from 4-6 rows of cells down to an array consisting of two rows of boundary contacting lateral cells and rare internal, bipolar cells by midneurula (Stage 15-16) (Fig. 4B). From there, the cells begin to spread laterally, become thinner in their anterior posterior dimension to form the “pizza-slice” stack of notochordal cells (Fig. 4B), which then take up water in vacuoles, thereby pressurizing a “hydrostat” (8). Meanwhile the surrounding matrix thickens and differentiates (133, 134). The notochord then straightens and elongates as a function of the pattern of its fiber-wound matrix (8, 135) and thereby contributes to the lifting, straightening and elongation of the tail (Fig. 1D,E). Mechanical models illuminate the relationship between the fiber-winding angle, hydrostatic pressure, and change in shape of the notochord (135). The epithelioid mode of intercalation with its broad panel of septin-confined, actomyosin activity (87, 88) (Fig. 3F) fits well with the transition to the circumferential spreading that forms the “pizza slice” cells, and highlights the importance of further work in this period, which involves further differentiation of matrix, including assembly and distribution of fibronectin, fibrillin, elastin, and laminin around the notochord (58, 59, 133) and the complex “adhesome” consisting of Dystroglycan (Dg), laminin, and myosin IIA, which functions in adhesion, actin organization, polarity, and finally, vacuolation (134), a key step in forming the pressurized fiber-wound hydrostat (135).

19. Late Endoderm Elongation.

Notochord straightening is accompanied by elongation of the vegetal endoderm on the ventral side (Fig. 1D, E), a process that has been attributed to the lateral plate mesoderm in *Xenopus* (19) and to the endoderm in urodeles (20). Explants and cell labeling experiments on the urodele (tailed) amphibian, *Ambystoma mexicanum*, shows that the vegetal endoderm actively elongates, a process requiring signals from the blastopore region (19). Fate mapping of *Xenopus* gut formation shows that the original archenteron is nearly lost due to closure and the endoderm forms the gut tube through subsequent outward radial intercalation of cells toward a “boundary capture” at the surrounding basal lamina (136, 137). Similar to the cell intercalation seen at the mesoderm and the neural tissue, this intercalation is Rho/ROCK/MyosinII and PCP (Vangl2) dependent, and it forms the definitive cavity and elongates the gut in one stroke (138–140; also see 141). This represents yet another example of the nearly omnipresent process of CE in early development.

20. CE as a large-scale mechanical patterning mechanism.

CE strains (stretches) tissues that otherwise do not show strain and thus shapes the embryo, but this strain is also used in patterning aspects of the embryo, how many is yet to be determined. The presumptive epidermis shows a pattern of strain toward the closing blastopore in the late gastrula and early neurula (9), and later in the tailbud stage, the epidermal multiciliated cells generate fluid flow along this pattern (142). This flow pattern that can be redirected by new micro-aspiration-induced strain, which regulates the polarity of the multiciliated cells in a stage specific manner and involving microtubule alignment and differential turnover of cell adhesion and PCP proteins (142). More striking, there is two-dimensional gradient of endogenous CE-generated strain in the posterior roof of the gastrocoel, the left-right organizer (LRO), which regulates the cell polarity, and the apical position, and length of the cilia responsible for LRO function in a strain-dependent manner (143). In both the epidermis and the LRO, the PCP pathway is necessary for strain-mediated patterning, but the essential, large scale coordinator is the pattern of mechanical strain. The key parameter in these experiments is cellular strain, and the tissue strain applied by large scale CE movements to other, passive tissues is translated into cellular strain by the cells' resistance to passive intercalation. As the tissue is strained, cells that slide by one another easily would passively rearrange and would show little or no cellular strain, whereas those that have higher resistance to passive rearrangement, will show cellular strain increasing in proportion to their resistance (see 144 for an excellent discussion). One could imagine that cells could differentiate resistance to rearrangement at specific developmental periods, to specific degrees, and in specific places, and thus produce a temporally and regionally specific cellular strain in response to a given tissue strain, and respond to this strain level with regulatory changes.

21. Outlook

Many advances have and are being made on understanding CE in *Xenopus* early development, the most significant ones being in resolving the cell biology and biomechanics of key underlying processes. Several problems stand out as challenging but important ones. The signaling processes that underlie the spatiotemporal progressions of MIB are key to understanding how the activities of large populations of cells are coordinated to produce the elegant sweep of MIB/CE across the embryonic landscape. Second, we know too little about the generation and magnitude of the forces that are contributed by the various tissues involved, particularly how local and global forces and mechanical properties are tuned to one another. Third, it seems likely that the forces generated by the progression of force-generating cellular processes and properties feed back, positively or negatively, to regulate their own progression and spatial patterning, and this needs to be understood. Fourth, it is important to understand the regulation of the radial and mediolateral cell behaviors and integration of the forces they generate during CE. Finally, it is important to understand that the specificity of morphogenic movements emerges from contextual information (mechanical and physiological) at many levels. Local force-cell behaviors can result in many different outcomes depending on their spatial pattern, their mechanical connectivity, their geometries, and their anchor points in the larger system. The old adage that the whole is greater than the sum of its parts has turned out to be so true.

References:

1. Lang M. Lighting up the mechanome; Frontiers of Engineering: Reports on Leading-Edge Engineering from the 2007 Symposium; Washington, DC: The National Academies Press; 2008. 39–47. .
2. Vogt W 1929 Gestaltanalyse am Amphibienkein mit ortlicher Vitalfarbung. II. Teil. Gastrulation und Mesodermbildung bei Urodelen und Anuren. Wilhelm Roux Arch. EntwMech. Org 120, 384–706.
3. Condic ML, Fristrom D, and Fristrom JW, 1991 Apical cell shape changes during *Drosophila* imaginal leg disc elongation: a novel morphogenetic mechanism Development 111, 23–33. [PubMed: 2015798]
4. Bissen ST and Weisblat DA 1989 The durations and compositions of cell cycles in embryos of the leech, *Helobdella triserialis*. Development 106, 105–118. [PubMed: 21428107]
5. Williams M and Solnica-Krezel L 2020 Cellular and molecular mechanisms of convergence and extension in zebrafish Sonica-Krezel L (Ed.), Current topics in developmental biology, Vol. 136 Elsevier Pp. 34–46.
6. Solnica-Krezel L, and Sepich DS (2012). Gastrulation: Making and shaping germ layers. Annual Review of Cell and Developmental Biology, Vol. 28, pp. 687–717.
7. Tuft PH, 1962 The uptake and distribution of water in the embryo of Xenopus laevis (Daudin). J. Exp. Biol 39, 1–19. [PubMed: 13923033]
8. Adams D, Keller R, Koehl M 1990 The mechanics of notochord elongation, straightening, and stiffening in the embryo of *Xenopus laevis*. Development 110, 115–130. [PubMed: 2081454]
9. Keller RE 1975 Vital dye mapping of the gastrula and neurula of *Xenopus laevis*. I. Prospective areas and morphogenetic movements of the superficial layer. Dev. Biol 42, 222–241. [PubMed: 46836]
10. Keller RE 1976 Vital dye mapping of the gastrula and neurula of Xenopus laevis. II. Prospective areas and morphogenetic movements of the deep layer. Dev. Biol 51, 118–137. [PubMed: 950072]
11. Keller RE and Tibbetts P 1989 Mediolateral cell intercalation in the dorsal axial mesoderm of *Xenopus laevis*. Dev. Biol, 131, 539–549 [PubMed: 2463948]
12. Keller R, Shih J, and Sater A 1992 The cellular basis of the convergence and extension of the *Xenopus* neural plate. Dev. Dyn 193, 199–217. [PubMed: 1600240]
13. Lane MC, Davidson L, and Sheets M 2004 BMP antagonism by Spemann's organizer regulates rostral-caudal fate of mesoderm. Dev. Biol 275, 356–374. [PubMed: 15501224]
14. Keller RE 1978 Time-lapse cinemicrographic analysis of superficial cell behavior during and prior to gastrulation in *Xenopus laevis*. J. Morph 157, 223–248. [PubMed: 30235909]
15. Wilson P, Oster G and Keller RE 1989 Cell rearrangement and segmentation in *Xenopus*: Direct observation of cultured explants. Development 105, 155–166. [PubMed: 2806114]
16. Keller RE , Cooper M, Danilchik M, Tibbetts P and Wilson P 1989 Cell intercalation during notochord development in *Xenopus laevis*. J. Exp. Zool 251, 134–154. [PubMed: 2769201]
17. Wilson P and Keller R 1991 Cell rearrangement during gastrulation of Xenopus: Direct observation of cultured explants. Development 112, 289–300 [PubMed: 1769334]
18. Keller R 1991 Early embryonic development of *Xenopus laevis*. Chapter 5. Methods in Cell Biology, Vol. 36, Xenopus laevis: Practical Uses in Cell and Molecular Biology (Kay B and Peng B, eds.) Academic Press, Inc pp. 61–113.
19. Larkin K and Danilchik M 1999 Ventral cell rearrangements contribute to the anterior-posterior lengthening between neurula and tailbud stages in Xenopus laevis. Dev. Biol 216, 550–560. [PubMed: 10642792]
20. Drawbridge J, Steinberg MS 2000 Elongation of axolotl tailbud embryos requires GPI-linked proteins and Organizer-Induced, active, ventral trunk endoderm cell rearrangements. Dev. Biol 223, 27–37. [PubMed: 10864458]
21. Gimlich R and Braun J 1985 Improved fluorescent compounds for tracing cell lineage. Dev. Biol 109, 509–514. [PubMed: 2581834]
22. Fristrom D 1976 The mechanism of evagination of the imaginal discs of Drosophila melanogaster. III. Evidence for cell rearrangement. Dev Biol. 54, 163–171. [PubMed: 825402]

23. Fristrom D 1982 Septate junctions in imaginal disks of Drosophila: A model for the redistribution of septa during cell rearrangement. J. Cell Biol 94, 77–87. [PubMed: 7119018]
24. Taylor J and Adler P 2008 Cell rearrangement and cell division during the tissue level morphogenesis of evaginating Drosophila imaginal discs. Dev. Biol 313, 739–751. [PubMed: 18082159]
25. Schechtman AM 1942 The mechanism of amphibian gastrulation. I. Gastrulation-promoting interactions between various region of an anuran egg (*Hyla regilla*). Univ. Calif. Publ. Zool 51, 1–39.
26. Keller and Danilchik, 1988 Regional expression, pattern and timing of convergence and extension during gastrulation of *Xenopus laevis*. Development 103, 193–209. [PubMed: 3197629]
27. Doniach T, Phillips CR, and Gerhart JC 1992 Planar induction of anteroposterior pattern in the developing central nervous system of Xenopus laevis. Science 257, 542–545. [PubMed: 1636091]
28. Poznanski A and Keller R 1997 The role of planar and early vertical signaling in patterning the expression of Hoxb-1 in Xenopus. Develop. Biol 184, 351–366. [PubMed: 9133441]
29. Shook DR, Wen J, Rolo A, Francica B, Dobins D, Skoglund P, DeSimone D, Winklbauer R, Keller R 2018 Characterization of convergent thickening, a major convergence force producing morphogenic movement in amphibians. BioRxiv. DOI: 10.1101/270892
30. Moore SW, Keller RE, and Koehl MAR 1995 The dorsal involuting marginal zone stiffens anisotropically during its convergent extension in the gastrula of Xenopus laevis. Development 121,3131–3140. [PubMed: 7588048]
31. Moore SW 1994 A fiber optic system for measuring dynamic mechanical properties of embryonic tissues. IEEE Trans Biomed Eng. 41,45–50. [PubMed: 8200667]
32. Zhou J, Kim HY, and Davidson LA 2009 Actomyosin stiffens the vertebrate embryo during crucial stages of elongation and neural tube closure. Development 136, 677–688. [PubMed: 19168681]
33. Wilson P 1991 The development of the axial mesoderm in *Xenopus laevis*. Ph.D. Thesis, University of Virginia, Charlottesville, VA
34. Shih J and Keller R 1992a Cell motility driving mediolateral intercalation in explants of *Xenopus laevis*. Development 116, 901–914. [PubMed: 1295743]
35. Shih J and Keller R 1992b Patterns of cell motility in the organizer and dorsal mesoderm of *Xenopus*. Development 116, 915–930. [PubMed: 1295744]
36. Davidson LA, Keller R and DeSimone DW 2004 Patterning and tissue movements in a novel explant of the marginal zone of *Xenopus laevis*. Gene Expression Patterns 4, 457–466. [PubMed: 15183313]
37. Keller R Danilchik M, Gimlich R and Shih J 1985 The function and mechanism of convergent extension during gastrulation of *Xenopus laevis*. J. Embryol. exp. Morph 89, Supplement, 185–209. [PubMed: 3831213]
38. Gillespie JI 1983 The distribution of small ions during the early development of *Xenopus laevis* and *Ambystoma mexicanum* embryos. J. Physiol 344, 359–77. [PubMed: 6655587]
39. Keller RE and Schoenwolf GC 1977 An SEM study of cellular morphology, contact, and arrangement, as related to gastrulation in *Xenopus laevis*. Wilhelm Roux's Arch. 182, 165–186.
40. Keller R 1984 The cellular basis of gastrulation in *Xenopus laevis*: active, postinvolution convergence and extension by mediolateral interdigitation. Amer. Zool 24, 589–603.
41. Goto T, Davidson LA, Asashima M, and Keller R 2005 Planar cell polarity genes regulate polarized extracellular matrix deposition during frog gastrulation. Curr. Biol 15, 787–793. [PubMed: 15854914]
42. Ossipova O, Chu C-W, Filatre J, Brott BK, Itoh K and Sokol SY 2014 The involvement of PCP proteins in radial cell intercalations during Xenopus embryonic development. Dev. Biol 408, 316–327.
43. Yen WW, Williams M, Periasamy A, Conaway M, Burdsal C, Keller R, Lu X, Sutherland A 2009 PTK7 is essential for polarized cell motility and convergent extension during mouse gastrulation. Development 136, 2039–2048. [PubMed: 19439496]
44. Shook D, 2015 Shook D, Kasprowicz EM, Davidson L, and Keller R 2018 Large long range tensile forces drive convergence, blastopore closure, and body axis elongation. eLife, 2018 3 13;7 pii: e26944. doi: 10.7554/eLife.26944. 10.7554/eLife.26944.001

45. Keller RE 1980 The cellular basis of epiboly: An SEM study of deep-cell rearrangement during gastrulation in *Xenopus la*evis. J. Embryol. exp. Morph 60, 201 [PubMed: 7310269]
46. Marsden M and DeSimone D 2001 Regulation of cell polarity, radial intercalation and epiboly in Xenopus: novel roles for integrin and fibronectin. Development 128, 3635–3647 [PubMed: 11566866]
47. Marsden M and DeSimone D 2003 Integrin-ECM Interactions Regulate Cadherin-Dependent Cell Adhesion and Are Required for Convergent Extension in *Xenopus*. Current Biology, Vol. 13, 1182–1191. [PubMed: 12867028]
48. Dzamba BJ, Jakab KR, Marsden M, Schwartz MA, and DeSimone DW 2009 Cadherin adhesion, tissue tension, and noncanonical Wnt signaling regulate fibronectin matrix organization. Dev. Cell, 16, 421–432. [PubMed: 19289087]
49. Damm EW and Winklbauer R 2011 PDGF-A controls mesoderm cell orientation and radial intercalation during *Xenopus* gastrulation. Development 138, 565–575. [PubMed: 21205800]
50. Szabo A, Cobo I, Omara S, McLachlan S, Keller R, and Mayor R 2016 The molecular basis of radial intercalation during tissue spreading in early development. Developmental Cell 37, 213–225. [PubMed: 27165554]
51. Ninomiya H, and Winklbauer R (2008) Epithelial coating controls mesenchymal shape change through tissue-positioning effects and reduction of surface-minimizing tension. Nat. Cell Biol 10:61–69. [PubMed: 18084283]
52. Longo D, Peirce SM, Skalak T, Davidson L, Marsden M, Dzamba B, and DeSimone D 2004 Multicellular computer simulation of morphogenesis: blastocoel roof thinning and matrix assembly in *Xenopus laevis*. Dev. Biol 271, 210–222. [PubMed: 15196962]
53. Keller R, Shih J and Domingo C 1992 The patterning and functioning of protrusive activity during convergence and extension of the *Xenopus* organizer. Development Supplement 1992, 81–91.
54. Keller R, Davidson R, Edlund A, Elul T, Ezin M, Shook D, and Skoglund P2000 Mechanisms of convergence and extension by cell intercalation. Phil. Trans. R. Soc. Lond. B 355, 897–922. [PubMed: 11128984]
55. Fagotto F, Rohani N, Touret A-S, Li R 2013 A molecular base for cell sorting at embryonic boundaries: contact Inhibition of cadherin adhesion by Ephrin/Eph-dependent contractility. Developmental Cell 27, 1–16. [PubMed: 24135226]
56. Reintsch W, Habring-Mueller A, Wang R, Schohl A and Fagotto F 2005 β-catenin controls cell sorting at the notochord-somite boundary independently of cadherin-mediated adhesion. J. Cell Biol 170, 675–686. [PubMed: 16103232]
57. Rosario T, DeSimone DW 2009 The extracellular matrix in development and morphogenesis: a dynamic view. Dev Biol 341, 126–140 [PubMed: 19854168]
58. Skoglund P, Dzamba B, Coffman CR, Harris W and Keller R 2006 *Xenopus* fibrillin is expressed in the organizer and is the earliest component of matrix at the developing notochord-somite boundary. Dev. Dyn 235, 1974–1983, P., Keller, fibrillin, [PubMed: 16607639]
59. Skoglund P and Keller R 2007 *Xenopus* fibrillin is required for convergence and extension. Dev. Biol 301, 404–416. [PubMed: 17027959]
60. Sokol SY 1996 Analysis of Dishevelled signaling pathways during *Xenopus* development. Curr. Biol 6, 1456–1467. [PubMed: 8939601]
61. Wallingford J, Rowning BA, Vogeli KM, Rothbacher U, Fraser S, and Harland R 2000 Dishevelled controls cell polarity during *Xenopus* gastrulation. Nature 405, 81–85. [PubMed: 10811222]
62. Tada M and Smith JC 2000 Xwnt is a target of *Xenopus* Brachyury: regulation of gastrulation movements via Dishevelled, but not through the canonical Wnt pathway. Development 127 2227–2238. [PubMed: 10769246]
63. Djiane A, Riou J, Umbhauer M, Boucaut J and Shi D (2000). Role of frizzled 7 in the regulation of convergent extension movements during gastrulation in *Xenopus laevis*. Development 127, 3091–3100 [PubMed: 10862746]
64. Darken RS, Scola AM, Rakeman AS, Das G, Mlodzik M and Wilson PA (2002). The planar polarity gene strabismus regulates convergent extension movements in *Xenopus*. EMBO J. 21, 976–985. [PubMed: 11867525]

65. Goto T and Keller R (2002). The planar cell polarity gene Strabismus regulates convergence and extension and neural fold closure in *Xenopus*. Dev. Biol 247, 165–181. [PubMed: 12074560]
66. Habas R, Kato Y, He X, 2001 Wnt/Frizzled activation of Rho regulates vertebrate gastrulation and requires a novel Formin homology protein Daam1. Cell 107, 843–854. [PubMed: 11779461]
67. Habas R, Dawid IB, He X, 2003 Coactivation of Rac and Rho by Wnt/Frizzled signaling is required for vertebrate gastrulation. Genes Dev. 17, 295–309 [PubMed: 12533515]
68. Shendo A 2018 Models of convergent extension during morphogenesis. WIREs Dev Biol 2018 7:e293 doi: 10.1002/Wdev.293“
69. Butler MT, and Wallingford JB 2017 Planar cell polarity in development and disease. Nat Rev Mol Cell Biol. 18: 375–388. doi:10.1038/nrm.2017.11. [PubMed: 28293032]
70. Heisenberg C-P, Tada M, Rauch G-J, Saude L, Concha M, Geisler R, Stemple DL, Smith JC, , and Wilson SW 2000 Siberblick/Wnt11 mediates convergent extension movements during zebrafish gastrulation. Nature 405, 76–81. [PubMed: 10811221]
71. Jessen JR Topczewski J, Bingham S, Sepich DS, Marlow F, Chandrasekhar A, and Solnica-Krezel L 2002 Zebrafish trilobite identifies new roles for Strabismus in gastrulation and neuronal movements. Nat Cell Biol. 4, 610–615. [PubMed: 12105418]
72. Glickman NS, Kimmel CB, Jones MA and Adams RJ 2003 Shaping the zebrafish notochord. Development 130, 873–887. [PubMed: 12538515]
73. Yen WW, Williams M, Periasamy A, Conaway M, Burdsal C, Keller R, Lu X, Sutherland A 2009 PTK7 is essential for polarized cell motility and convergent extension during mouse gastrulation. Development 136, 2039–2048. [PubMed: 19439496]
74. Williams M, Yen W, Lu X, and Sutherland A 2014 Distinct apical and basolateral mechanisms drive planar cell polarity-dependent convergent extension of the mouse neural plate. Dev. Cell 29, 34–46. [PubMed: 24703875]
75. Davidson L, Marsden M, Keller R and DeSimone D 2006 Integrin α5β1 and fibronectin regulate polarized protrusions required for *Xenopus* convergence and extension. Curr. Biol 16, 833–844 [PubMed: 16682346]
76. Skoglund P, Rolo A, Chen X, Gumbiner B and Keller R 2008 Convergence and extension at gastrulation requires a myosin IIB dependent cortical actin network. Development 135: 2435–2444. [PubMed: 18550716]
77. Pfister K, Shook D, Chang C, Keller R, and Skoglund P 2016 Molecular model for force production and transmission during vertebrate gastrulation. Development 143, 715–727. [PubMed: 26884399]
78. Brieher W and Gumbiner B 1994 Regulation of C-cadherin function during activin induced morphogenesis of *Xenopus* animal caps. J. Cell Biol 126, 519–527 [PubMed: 8034750]
79. Kim HY, and Davidson LA 2011 Punctuated actin contractions during convergent extension and their permissive regulation by the non-canonical Wnt-signaling pathway. J. Cell Sci, 124, 635–646. [PubMed: 21266466]
80. Davidson L, Keller R, DeSimone D 2004 Assembly and remodeling of the fibrillar fibronectin extracellular matrix during gastrulation and neurulation in Xenopus laevis. Dev. Dyn 231:888–895. [PubMed: 15517579]
81. Rosario T, Dzamba B, Weber G, Davidson L and DeSimone D 2009 The physical state of fibronectin matrix differentially regulates morphogenetic movements in vivo. Dev. Biol 327, 386–398. [PubMed: 19138684]
82. Elul T, Koehl M and Keller R 1997 Cellular mechanism underlying neural convergent extension in *Xenopus laevis* embryos. Dev. Biol 191, 243–258. [PubMed: 9398438]
83. Elul T and Keller R 2000 Monopolar Protrusive Activity: A new morphogenic cell behavior in the neural plate dependent on vertical Interactions with the mesoderm in Xenopus. Dev. Biol 224, 3–19. [PubMed: 10898957]
84. Kelley C, Sellers J, Gard D, Bui D, Adelstein R and Baines I Xenopus nonmuscle myosin heavy chain Isoforms have different subcellular localizations and enzymatic activities. J. Cell Biol 134, 675–687. [PubMed: 8707847]
85. Rochlin MW, Itoh K, Adelstein R and Bridgman P 1995 Localization of myosin II A and B isoforms in cultured neurons. J. Cell Sci 108, 3661–3670. [PubMed: 8719872]

86. Zhou J, Pal S, Maiti S, and Davidson LA 2015 Force production and mechanical accommodation during convergent extension. Development 142, 692–701. [PubMed: 25670794]
87. Shindo A, Wallingford JB 2014 PCP and septins compartmentalize cortical actomyosin to direct collective cell movement. Science 343:649–652. [PubMed: 24503851]
88. Kim SK, Shindo A, Park TJ, Oh E, Ghosh S, Gray R, Lewis RA, Johnson CA, Attie-Tittach T, Katsanis N, Wallingford JB 2010 Planar Cell Polarity acts through septins to control collective cell movement and ciliogenesis. Science 329 1337–1340. [PubMed: 20671153]
89. Huebner RJ and Wallingford JB 2019 Coming to consensus: A unifying model emerges for convergent extension. Dev. Cell 46, 389–396
90. Discher D, Janmey P, Wang Y-L 2005 Tissue cells feel and respond to the stiffness of their substrate. Science 310, 1139–1143 DOI: 10.1126/science.1116995 [PubMed: 16293750]
91. Engler AJ, Sen S, Sweeney HL and Discher DE 2006 Matrix elasticity directs stem cell lineage specification. Cell 126, 677–689. [PubMed: 16923388]
92. Liua Z, Tanb JL, Cohena DM, Yanga MT, Sniadeckia NJ, Ruiza SA, Nelson CM, and Chen CS 2010 Mechanical tugging force regulates the size of cell-cell junctions. PNAS 107, 9944–9949. [PubMed: 20463286]
93. Barriga E, Franze K, Charras G Mayor R 2018 Tissue stiffening coordinates morphogenesis by triggering collective cell migration *in vivo*. Nature 554, 523–527. doi:10.1038/nature25742 Epub 2018 Feb 14. [PubMed: 29443958]
94. Blankenship JT, Backovic ST, Sanny JSP, Weitz O, Zallen JA 2006 Multicellular rosette formation links planar cell polarity to tissue morphogenesis. Dev Cell 11:459–470. [PubMed: 17011486]
95. Levayer R and Lecuit T 2013 Oscillation and polarity of E-Cadherin asymmetries control actomyosin flow patterns during morphogenesis. Dev. Cell 26, 162–175. [PubMed: 23871590]
96. Williams-Masson EM, Heid PJ, Lavin CA, and Hardin J 1998 The cellular mechanisms of epithelial rearrangement during morphogenesis of Caenorhabditis elegans dorsal hypodermis. Dev. Biol 204, 263–276. [PubMed: 9851858]
97. Sun Z, Amourda C, Shagirov M, Hara Y, Saunders TE, and Toyama Y 2017 Basolateral protrusion and apical contraction cooperatively drive Drosophila germ-band extension, Nat. Cell Biol 19 375–383. doi:10.1038/ncb3497. [PubMed: 28346438]
98. Brodland GW 2006 Do lamellipodia have the mechanical capacity to drive convergent extension. Int. J. Dev. Biol 50: 151–155. [PubMed: 16479484]
99. Belmonte JM, Swat MH, Glazier JA 2016 Filopodial-Tension Model of Convergent-Extension of Tissues. PLoS Comput Biol 12(6): e1004952. doi:10.1371/journal.pcbi.1004952 [PubMed: 27322528]
100. Jacobson AG and Gordon R 1976 Changes in the shape of the developing vertebrate nervous system analyzed experimentally, mathematically, and by computer simulation. J. Exp. Zool197, 191–246. [PubMed: 965908]
101. Lane MC and Keller R 1997 Microtubule disruption reveals that Spemann's organizer is subdivided into two domains by the vegetal alignment zone. Development 124, 895–906. [PubMed: 9043070]
102. Luxardi G, Marchal L, Thomé V and Kodjabachian L 2010 Distinct *Xenopus* Nodal ligands sequentially induce mesendoderm and control gastrulation movements in parallel to the Wnt/PCP pathway. Development 137, 417–426. [PubMed: 20056679]
103. Keller R and Shook D 2004 Gastrulation in amphibians In Gastrulation (ed. Stern C), Cold Spring Harbor Laboratory Press, NY
104. Wacker S Grimm K, Winklbauer R, Joos T and Winklbauer R 2000 Development and control of tissue separation at gastrulation in *Xenopus*. Dev. Biol 224, 428–439. [PubMed: 10926778]
105. Olivia Luu O, Erich W Damm EW, Parent SE, Barua D, Smith THL, Wen J, Lepage LE, Nagel M Huang Y, Bruce A, Ibrahim-Gawel H, and Winklbauer R 2015 PAPC mediates self/non-self-distinction during Snaill-dependent tissue separation J. Cell Biol 208, 839–856 www.jcb.org/cgi/doi/10.1083/jcb.201409026 [PubMed: 25778923]
106. Medina A, Swain R, Kuerner K-M, Steinbeisser H 2004 Xenopus paraxial protocadherin has signaling functions and is involved in tissue separation. EMBO J 23: 3249–3258. [PubMed: 15272309]

107. Winklbauer R Medina A, Swan RK, Steinbeisser H 2001 Frizzled-7 signaling controls tissue separation behavior during *Xenopus* gastrulation. Nature 413, 856–860. [PubMed: 11677610]
108. Rohani N, Canty L, Luu O, Fagotto F, Winklbauer R (2011) EphrinB/EphB Signaling Controls Embryonic Germ Layer Separation by Contact-Induced Cell Detachment. PLoS Biol 9(3): e1000597. doi:10.1371/journal.pbio. [PubMed: 21390298]
109. Domingo C and Keller R 1995 Induction of notochord cell intercalation behavior and differentiation by progressive signals in the gastrula of *Xenopus laevis* Development 121,3311–3321. [PubMed: 7588065]
110. Branford WW and Yost HJ 2002 Lefty-Dependent Inhibition of Nodal- and Wnt-Responsive Organizer Gene Expression Is Essential for Normal Gastrulation Curr. Biol 12, 2136–214 [PubMed: 12498689]
111. Ninomiya H, Elinson RP, and Winklbauer R 2004 Antero-posterior tissue polarity links mesoderm convergent extension to axial patterning. Nature 430, 364–367. [PubMed: 15254540]
112. Kwan KM, and Kirschner MW A microtubule-binding Rho-GEF controls cell morphology during convergent extension of *Xenopus laevis*. Development 132, 4599–4610. [PubMed: 16176947]
113. Kao KR and Elinson RP 1988 The entire mesodermal mantle behaves as Spemann's Organizer in dorsoanterior enhanced embryos. Devel. Biol 127, 64–77. [PubMed: 3282938]
114. Flournoy C 2009 Anterior-osterior tissue positional identity and anterior-posterior cell polarity maintain the axis of cell intercalation during *Xenopus* convergent extension. Ph.D. Thesis, University of Virginia, Charlottesville.
115. Shindo A, Inoue Y, Kinoshita M, Wallingford JB 2019 PCP-dependent transcellular regulation of actomyosin oscillation facilitates convergent extension of vertebrate tissue. Dev. Biol doi:10.1016/j.ydbio.2018.12.017.
116. Lane MC, Sheets MD, 2000 Designation of the anterior/posterior axis in pregastrula *Xenopus laevis*. Dev. Biol 225, 37–58. [PubMed: 10964463]
117. Lane MC and Sheets MD 2006 Heading in a new direction: Implications of the revised fate map for understanding Xenopus laevis development. Dev. Biol 296 12–28. [PubMed: 16750823]
118. Keller R, Shih J, Sater A, and Moreno C 1992 Planar induction of convergence and extension of the neural plate by the organizer of Xenopus. Dev. Dyn 193, 218–234. [PubMed: 1600241]
119. Butler MT, and Wallingford JB 2018 Spatial and temporal analysis of PCP protein dynamics during neural tube closure. eLife 2018;7:e36456 DOI: 10.7554/eLife.36456 [PubMed: 30080139]
120. Wallingford JB and Harland RM 2001 *Xenopus* Dishevelled signaling regulates both neural and mesodermal convergent extension: parallel forces elongating the body axis. Development 128, 2581–2592. [PubMed: 11493574]
121. Wallingford J and Harland R 2002 Neural tube closure requires Dishevelled-dependent convergent extension of the midline. Development 129, 5815–5825 (2002) 5815–5825 [PubMed: 12421719]
122. Ossipova1 O Kim K, Lake BB, Itoh K, loannou K, Sokol SY 2014 Role of Rab11 in planar cell polarity and apical constriction during vertebrate neural tube closure. Nat. Comm 5, 3734 | DOI: 10.1038/ncomms473410.1038/ncomms4734www.nature.com/naturecommunicationwww.nature.com/naturecommunication .
123. Elul T and Keller R 2000 Monopolar protrusive activity: a new morphogenic cell behavior in the neural plate dependent on vertical interactions with the mesoderm in *Xenopus*. Dev. Biol 224, 3–19. [PubMed: 10898957]
124. Jacobson AG, and Moury JD 1995 Tissue boundaries and cell behavior during neurulation. Dev. Biol 171,98–110. [PubMed: 7556911]
125. Ezin AM, Skoglund P, and Keller R 2003 The midline (notochord and notoplate) patterns the cell motility underlying convergence and extension of the *Xenopus* neural plate. Dev. Biol 256, 100–113. [PubMed: 12654295]
126. Ezin AM, Skoglund P and Keller R 2006 Presumptive floor-plate (notoplate) induces behaviors associated with convergent extension in medial but not lateral neural plate cells of *Xenopus*. Dev. Biol 300, 670–686. [PubMed: 17034782]
127. Keller RE 1981 An experimental analysis of the role of bottle cells and the deep marginal zone in gastrulation of *Xenopus laevis*. J. Exp. Zool 216, 81–101. [PubMed: 7288390]

128. Feroze R, Shawky JH, von Dassow M, and Davidson LA 2015 Mechanics of blastopore closure during amphibian gastrulation. Devel. Biol 398, 5767.

129. Schroeder TE 1970 Neurulation in *Xenopus laevis*. An analysis and model based on light and electron microscopy. Embryol. exp. Morph 23, 427–462.

130. Shawky JH, Balakrishnan UL, Stuckenholz C, and Davidson LA 2018 Multiscale analysis of architecture, cell size and the cell cortex reveals cortical F-actin density and composition are major contributors to mechanical properties during convergent extension. Development 145, dev161281. doi:10.1242/dev.161281

131. Zhou J, Pal S, Maiti S, Davidson LA 2015 Force production and mechanical accommodation during convergent extension. Development 142, 692–701. [PubMed: 25670794]

132. Collinet C, Rauzi M, Lenne P-F, Lecuit T 2015 Local and tissue-scale forces drive oriented junction growth during tissue extension. Nat. Cell Biol 17, 1247 [PubMed: 26389664]

133. Trapani V, Bonaldo P, Corallo D 2017 Role of the ECM in notochord formation, function and disease. J. Cell Science 130, 3203–3211 doi:10.1242/jcs.175950 [PubMed: 28883093]

134. Buisson N, Sirour C, Moreau N, Denker E, Bouffant R, Goullancourt A, Darribere T, Bello V 2014 An adhesome comprising laminin, dystroglycan and myosin IIA is required during notochord development in Xenopus laevis. Development 141,4569–4579. [PubMed: 25359726]

135. Koehl MAR, Quillin KJ, and Pell CA 2000 Mechanical design of fiber-wound hydraulic skeletons: the stiffening and straightening of embryonic notochords. Am. Zool 40, 28–41.

136. Chalmers AD and Slack JM 2000 The *Xenopus* tadpole gut: fate maps and morphogenetic movements. Development 127, 1457–1466.

137. Chalmers AD and Slack JM 1998 Development of the gut in *Xenopus laevis*. Dev. Dyn 212:509–521. [PubMed: 9707324]

138. Reed RA Womble MA Dush MK, Tull RR, Bloom SK, Morckel AR Devlin EW, and Nascone-Yoder NM 2009 Morphogenesis of the primitive gut tube Is generated by Rho/ROCK/Myosin II-mediated endoderm rearrangements. Dev. Dyn 238:3111–3125. [PubMed: 19924810]

139. Dush MK, and Nascone-Yoder NM 2019 Vangl2 coordinates cell rearrangements during gut elongation. Dev. Dyn 248, 569–582. [PubMed: 31081963]

140. Dush MK and Nascone-Yoder NM 2013 Jun N-terminal kinase maintains tissue integrity during cell rearrangement in the gut. Development 140, 1457–1466. [PubMed: 23462475]

141. Chung M-I, Nascone-Yoder NM, Grover SA, Drysdale TA, Wallingford JB 2010 Direct activation of Shroom3 transcription by Pitx proteins drives epithelial morphogenesis in the developing gut. Development 137, 1339–1349. [PubMed: 20332151]

142. Chien YH, Keller R, Kintner C, Shook DR 2015 Mechanical strain determines the axis of planar polarity in ciliated epithelia. Curr Biol. 25, 2774–2784. [PubMed: 26441348]

143. Chien Y-H, Srinivasan S, Keller R and Kintner C 2018 Mechanical strain determines cilia, length, motility and planar position in the left-right organizer. Dev. Cell 45, 316–330.e4. doi: 10.1016/j.devcel.2018.04.007. [PubMed: 29738711]

• 144. Blanchard GB, Kabla AJ, Schultz NL, Butler LC, Sanson B, Gorfinkiel N, Mahadevan L, and Adams RJ 2009 Tissue tectonics: morphogenetic strain rates, cell shape change and intercalation. Nat. Methods 6, 458–464. [PubMed: 19412170]

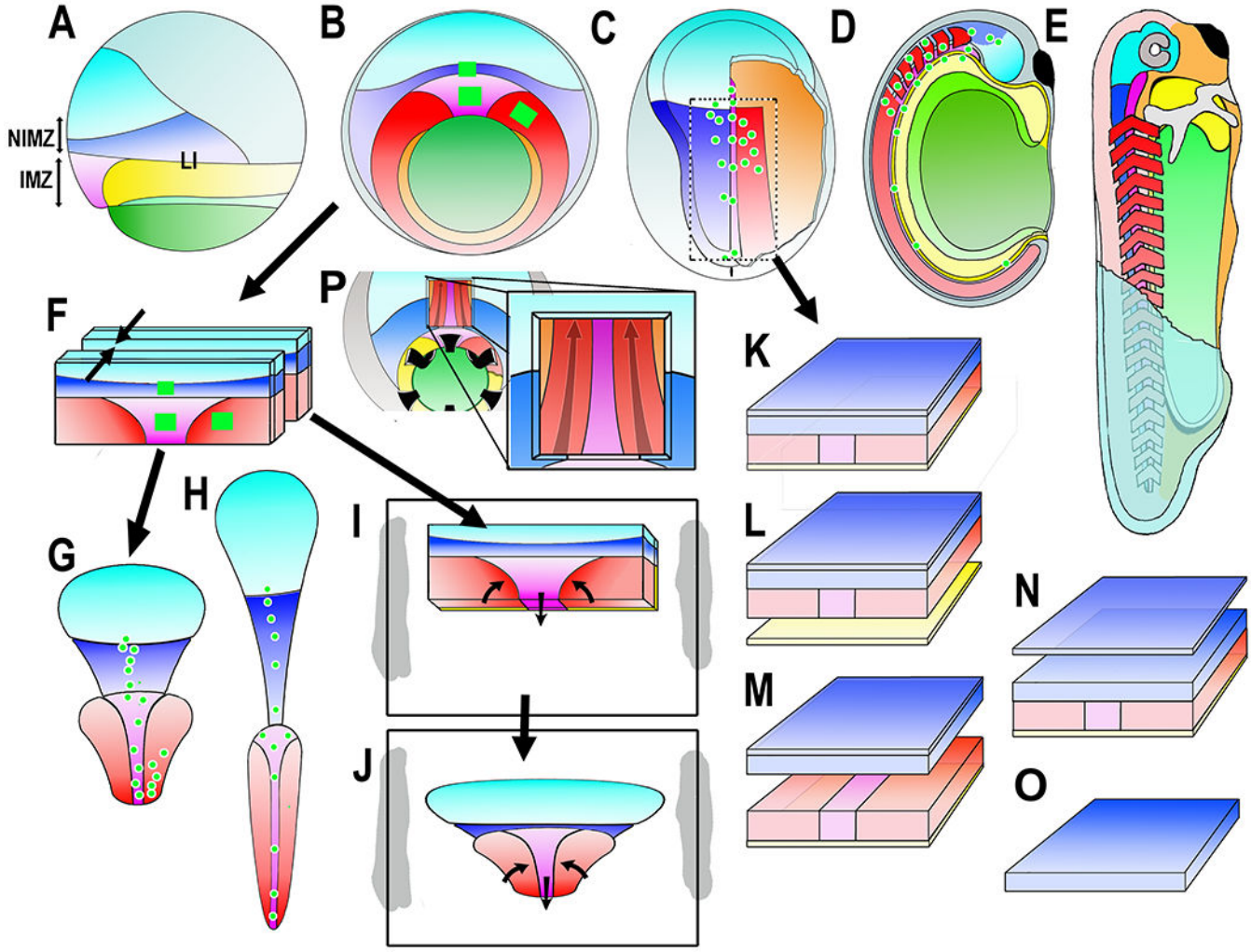

Figure 1.

Diagrams show the Xenopus early gastrua fate map in lateral (A) and vegetal (B) views, the early neurula in dorsal view, right side cutaway to show postinvolution mesoderm (C), the closed neural tube stage in sagittal view (D), and the early tadpole in a cutaway view (E). Ectodermal fates are: epidermis (dull blue), forebrain (bright blue), and hindbrain/spinal cord (dark blue). Mesodermal fates are: notochord (magenta), somitic mesoderm (red), head, heart and lateroventral mesoderm (orange). Endodermal fates are: archenteron roof suprablastoporal endoderm (yellow, removed to show underlying mesoderm in B and explants (F-J), archenteron roof/bottle cell endoderm (light green), and vegetal endoderm (dark green). The future anterior-posterior (A-P) axes are shaded from A (dark) to P (light). Also indicated are the IMZ (Involuting Marginal Zone), the NIMZ (Non-Involuting Marginal Zone), and the LI (Limit of Involution). Construction of experimental preparations are shown for the “Keller Sandwich” (F-G-H), the Open-faced explant as made (F-I) and undergoing convergent extension (J), the “dorsal isolate” or “Wilson explant (C-K), with endodermal epithelium removed to reveal deep notochordal and somitic mesoderm (L), with neural and mesodermal separated to reveal their apposing surfaces (M), with epithelial neural removed to reveal deep neural with underlying mesoderm (N), and isolated neural

deep layer (O), and the Davidson “windowed” embryo to reveal deep notochordal and somitic mesoderm (P). The square green patches and green dots are schematic representations of the graded separation of labeled patches of cells during convergent extension.

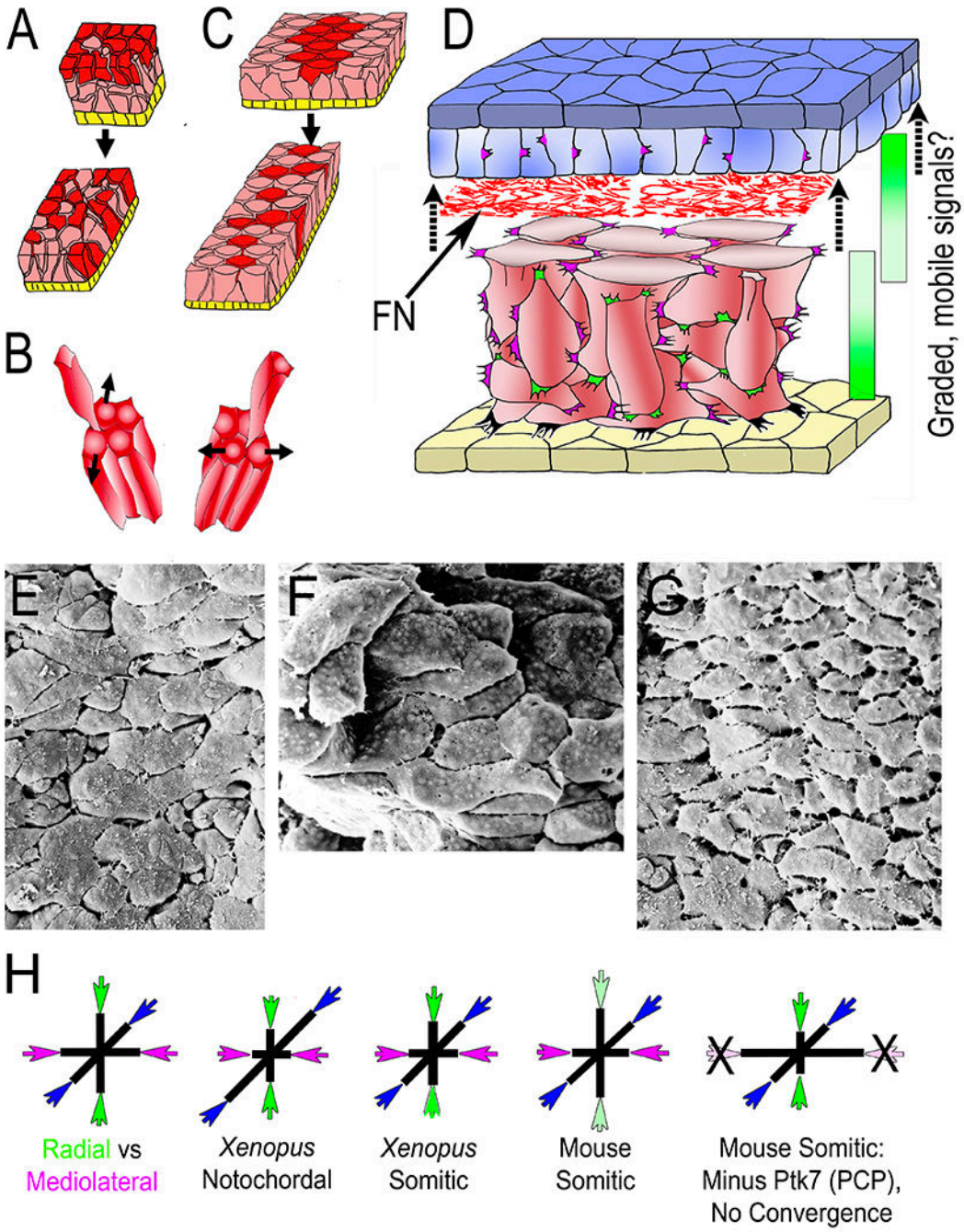

Figure 2.

Diagrams illustrate intercalation of deep mesodermal cells along the radial axis of the embryo (normal to the surface epithelium (yellow), designated Radial Intercalation (RI) (A), and their intercalation mediolaterally (across the future body axis) designated mediolateral intercalation (MI), together, resulting in convergent extension (CE). In this case, RI is biased to occur between anterior and posterior neighbors (B, left) rather than between medial and lateral neighbors (B, right). The context and details of RI and MI during early CE are illustrated in D, showing the overlying presumptive neural tissue (epithelial layer, dark blue;

deep layer light blue), a network of fibronectin fibrils (FN) between the basal layer of the presumptive neural tissue and outer layer of the deep mesodermal cells (red), which show mediolaterally polarized protrusive activity, reflective of intercellular traction and development of mediolateral tensile stress (magenta), and radially polarized protrusive activity acting orthogonally (green). At later stages FN is also assembled at the interface of the deep mesoderm and the overlying epithelial roof of the gastrocoel/archenteron (yellow). Integrin-FN signaling is essential for RI, as are mobile, chemotactic, signaling molecules (C3, PDGFA) two other tissues in early *Xenopus* embryos, raising the possibility in this tissue. Scanning electron micrographs of the late gastrula notochord in dorsal (E) and transverse (F) view, and the somitic mesoderm in dorsal view (G). The Tri-axial Force Model of tissue shaping (H) show the postulated relationship between radial (green), and mediolateral (magenta) forces overcoming the resistance to extension in the third, A-P axis (blue) to varying, tissue-specific degrees in the *Xenopus* notochord and somitic mesoderm. Experimental support for tri-axial tissue molding forces comes from dramatic flattening and widening of mouse somitic mesoderm after loss of convergence forces.

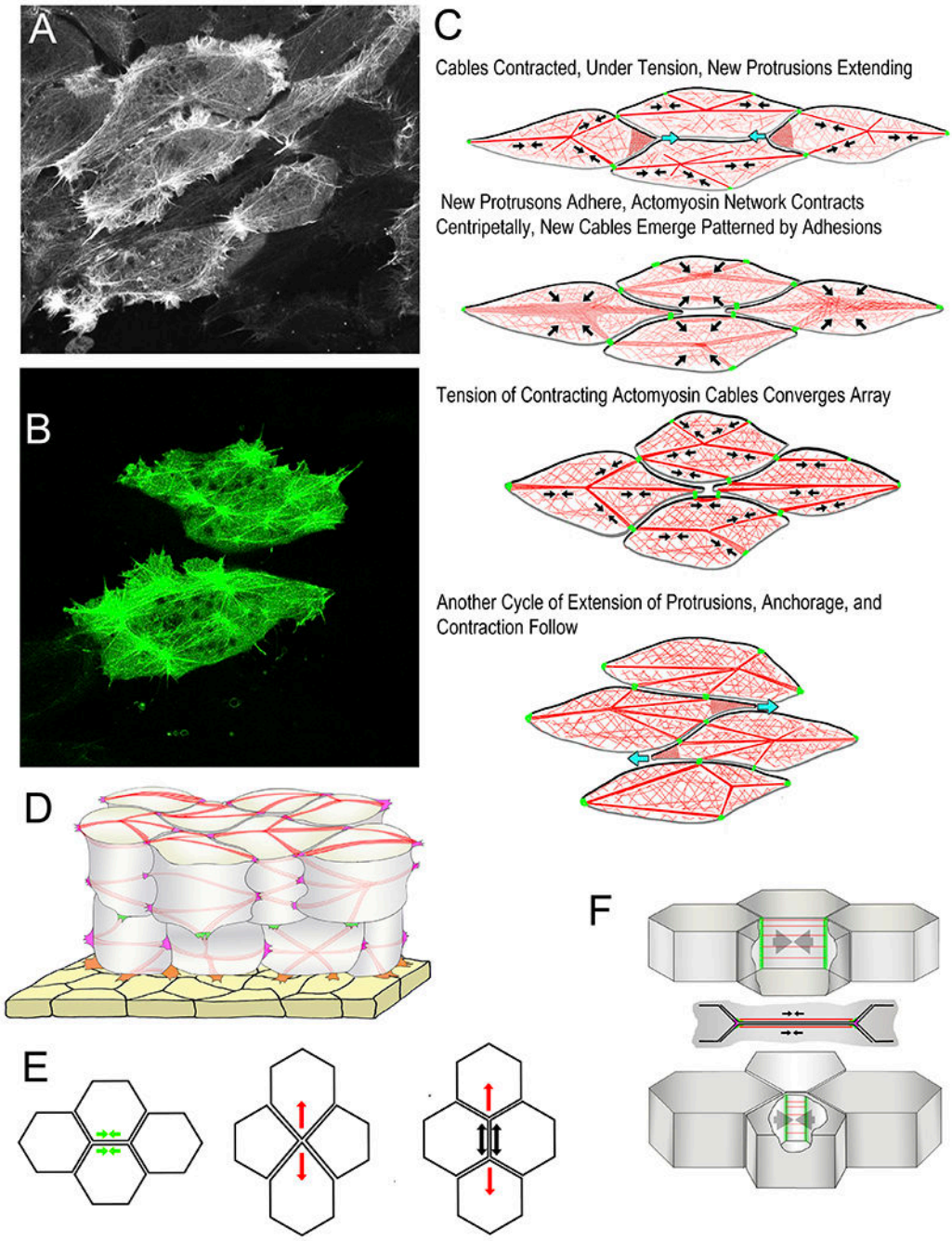

Figure 3.

Scanning laser confocal micrographs from time-lapse movies show examples of the Node and Cable Network (NCN) actin cytoskeleton with Moesin-AB-GFP (A, B). Diagrams show phases of Mediolateral Intercalation Behavior (MIB) in the Cell-on-Cell Traction Model of intercalation (C). Black arrows indicate contraction of F-actin network/F-actin cables (red), green indicates C-cadherin adhesions, and blue arrows indicate extension of protrusions. Anterior sides of cells are black, the posterior gray. A semitransparent diagram shows surface cables and lateral cables of the cortical NCN (red) anchored to mediolateral

(magenta) and radial (green) tractive protrusions, and protrusions connected to the underside of the epithelial endoderm of the archenteron roof (yellow). An illustration of the Epithelial Junctional Remodeling mode of epithelial cell intercalation (E) shows the initial active contraction (green arrow), or junction shortening (left), the formation of the tetrad of cells meeting a point, and the initiation of “resolution” with a centripetal contraction of the actomyosin cytoskeleton of the same cells (red arrows, middle), and the completed intercalation (right) showing the active contraction of resolution (red arrows) and the passive response of the intercalated cells (black arrows) (based on reference 132). A diagram shows the features of the junction shortening step of the epithelial-type intercalation behavior of notochord cells (F). Septins (green) form barriers that confine the active myosin to the actomyosin cables (red) of the cortical regions of the two apposed cell boundaries (in lateral view, top, and vertical view, middle); contraction of actomyosin cables shortens the boundaries (arrows) until the vertices meet (bottom). Based on reference (89).

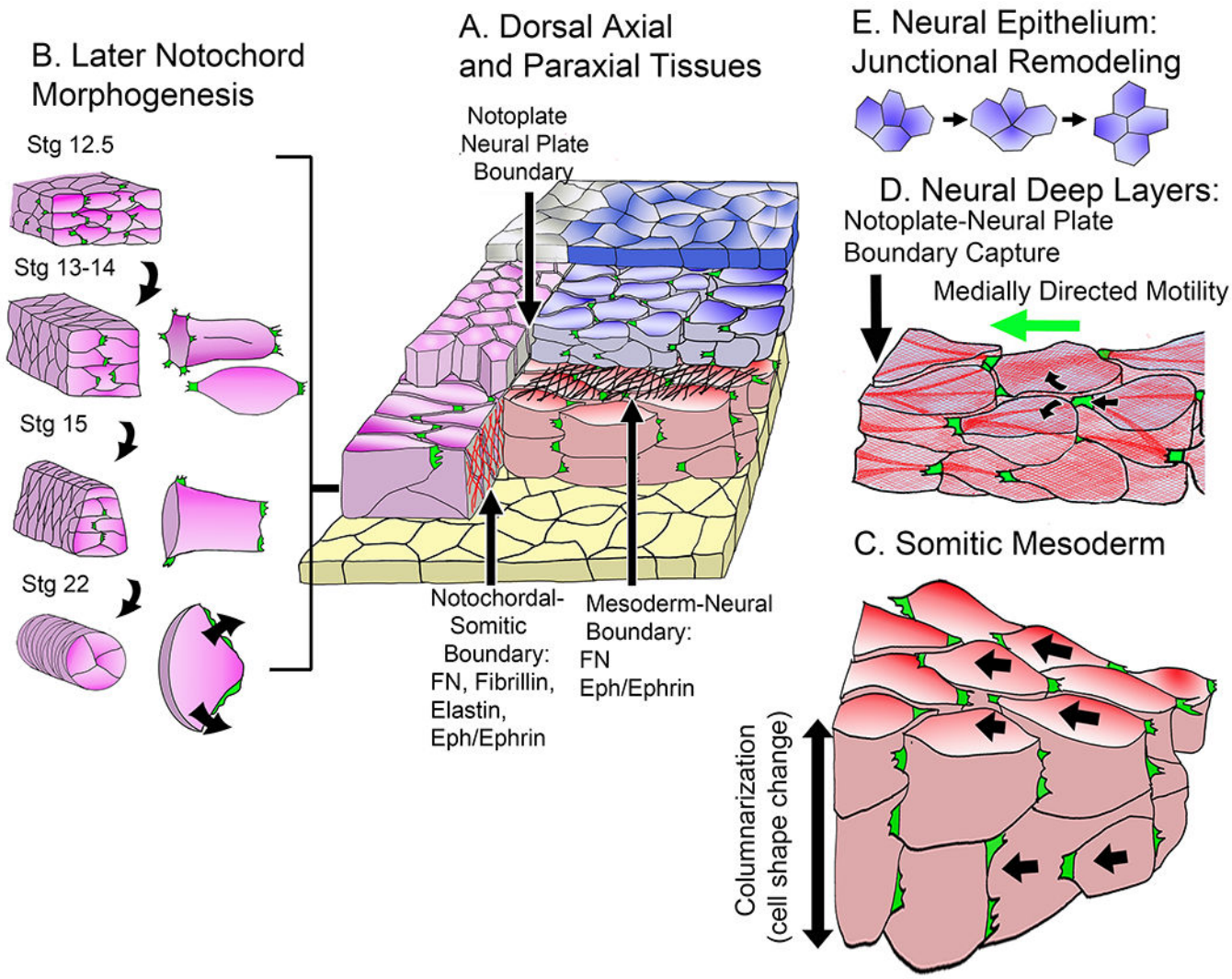

Figure 4.

A diagram (A) shows relationships in the early neurula between notochord (magenta), the deep layer notoplate of the neural plate above it (magenta), the epithelial layer of the notoplate (gray), the somitic mesoderm (red), the deep layer of the neural plate (blue-gray), the epithelial layer of the neural plate (blue) and the endodermal gastrocoel (archenteron) roof (yellow). Diagrams (B) show differentiation of new patterns of MIB at Nieuwkoop-Faber developmental stages (magenta): 1) the transition from a mix of bipolar protrusive activity of internal cells and monopolar, inwardly directed protrusive activity of boundary cells (Stage12.5 to Stage 14) and the transition from monopolar inwardly directed protrusive activity to circumferential spreading, forming pizza-slice shaped cells, and rounding of the notochord at the onset of vacuolation (Stage 15 to Stage 22) (16). A diagram (C) shows convergence of the presomitic mesoderm by the bipolar mode of intercalation in the now double-layered somitic mesoderm, which is later accompanied by columnarization of the medial somitic mesoderm, the second component of somitic convergence. A diagram (D) shows the medially directed monopolar protrusive activity and crawling mode of intercalation in the deep neural layer, using actomyosin cables similar to those seen in the

notochordal and somitic mesoderm. A diagram (E) illustrates the Epithelial Junctional Remodeling (EJR) mode of cell intercalation characteristic of the outer neural epithelial layer (119).

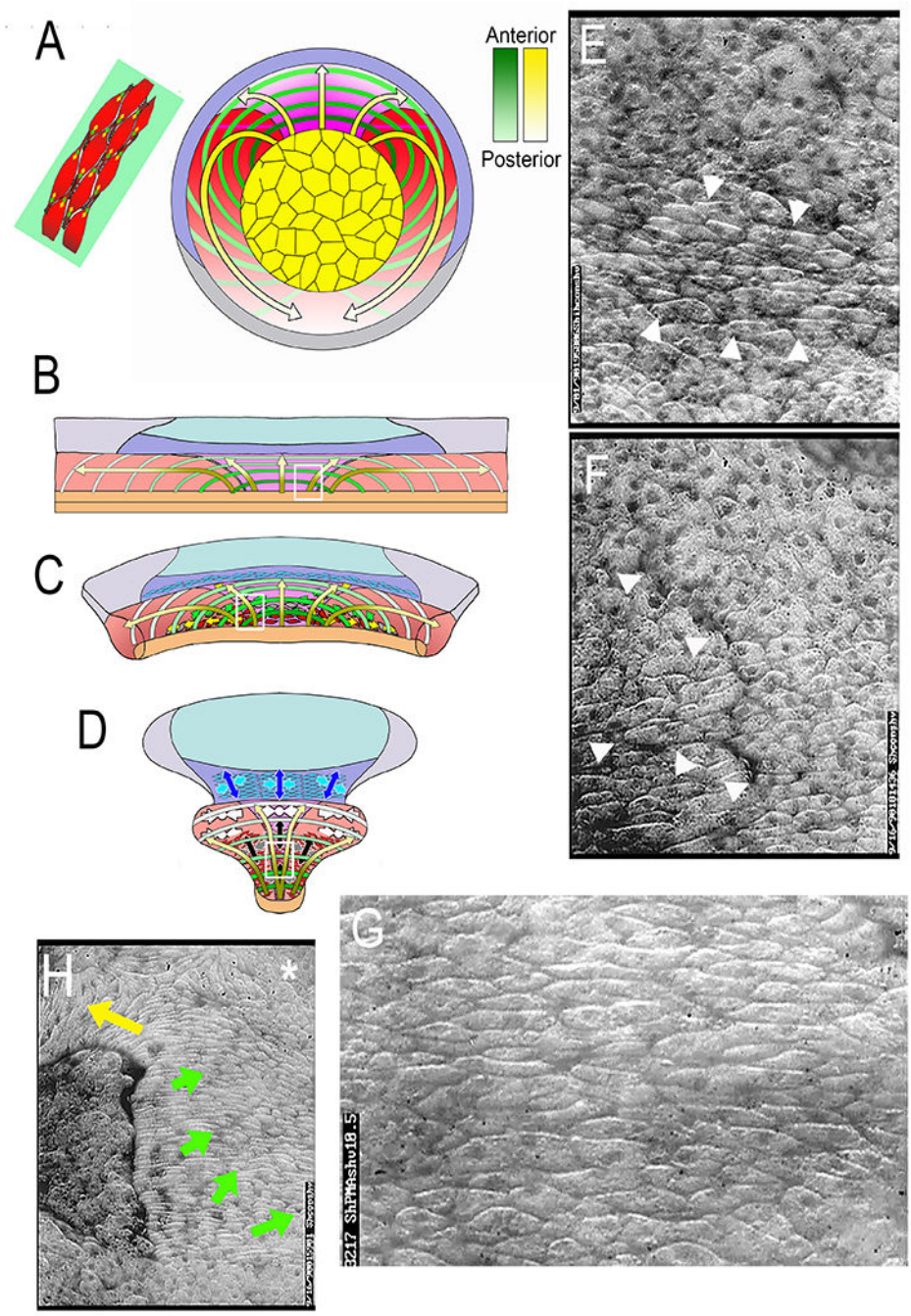

Figure 5.

The spatiotemporal pattern of expression of mediolateral intercalation behavior (MIB) is a continuous progression from presumptive anterior (yellow arrows, dark ends) to presumptive posterior (yellow arrows, light ends) mapped on to the IMZ (A). It occurs in an arc like pattern, here illustrated as discrete hoops progressing from early and anterior (dark green) to late and posterior (light green); each hoop is anchored at the vegetal endoderm (yellow), and represents an arc of intercalating deep mesodermal cells (upper left (A); The arcs are pushed toward the blastoporal lip by preinvolution CT (Convergent Thickening) and as they involute

the arcs shorten in A-P order with the expression of MIB, thereby pulling the archenteron roof and dorsal, somitic and notochordal mesoderm over the vegetal endoderm and closing the blastopore. This pattern was determined by mapping the expression pattern of MIB in large open-faced explants on to the IMZ (B) where A-P progressive arc-shortening results in CE (C-D). Images from low angle epi-illuminated open-faced explants show key features: the early onset of MIB in the vegetal alignment zone at Stg 10.5 (arrow heads in E, and white box in B); the initial, focal formation and subsequent straightening of the notochordal-somitic mesodermal boundary through the intercalating cells of the VAZ shortly thereafter (arrow heads in F, white box in C), a large, elongated, aligned and intercalating population of cells in the early central notochordal field (G, and white box in D). and a late neurula/early tailbud explant in which CE was retarded with excessive coverslip pressure, which results in partial progression of MIB and the subsequent vacuolation of the notochodal cells (G). Note the progression of vacuolation from the lateral boundary of the notochord posteriorly (yellow arrow) and medially from this lateral origin (green arrow), and undifferentiated, blebbing, rounded cells at the posterior medial notochordal field (asterisk). See references 34 and 35.